From the Klinik für Experimentelle Tumorforschung
(Director: Prof. Dr. Susanne Sebens)
at the University Medical Center Schleswig-Holstein, Campus kiel
at Kiel University

NEAR-INFRARED FLUORESCENT IMAGING OF PANCREATIC CANCER IN MICE USING A NOVEL ANTIBODY TO CEACAM5

Dissertation
to acquire the doctoral degree (Dr. med.)
at the Faculty of Medicine
at Kiel University

presented by
XILE ZHOU
from LanXi, Zhejiang, P.R China
Kiel 2021

From the Klinik für Experimentelle Tumorforschung
(Director: Prof. Dr. Susanne Sebens)
at the University Medical Center Schleswig-Holstein, Campus kiel
at Kiel University

NEAR-INFRARED FLUORESCENT IMAGING OF PANCREATIC CANCER IN MICE USING A NOVEL ANTIBODY TO CEACAM5

Dissertation
to acquire the doctoral degree (Dr. med.)
at the Faculty of Medicine
at Kiel University

presented by
XILE ZHOU
from LanXi, Zhejiang, P.R China
Kiel 2021

1st Reviewer: Prof. Dr. rer. nat. Holger Kalthoff

2nd Reviewer: Prof. Dr. Thomas Becker

Date of oral examination: 25.03.2021

Approved for printing, Kiel,

Signed:

INDEX

Abbreviations

CEACAM	Carcinoembryonic Antigen-related Cell Adhesion Molecules
PSG	Glycine rich glycoprotein
FMT	fluorescence molecular tomography
FITC	fluorescein isothiocyanate
FACS	Fluorescence Activating Cell Sorter
FCM	flow cytometry
MRI	magnetic resonance imaging
PET	positron emission tomography
SPECT	single photon emission computed tomographic
NIR	Near-infrared
NIRF	Near-infrared fluorescence
CT	computer tomography
ICG	Indocyanine Green
PDAC	pancreatic ductal adenocarcinoma
ISOBM	International Society for Cancer Developmental Biology and Medicine
GPI	Glycosylphosphatidylinositol
LPS	lipopolysaccharide
IC50	half-maximal inhibitory concentration
QDs	quantum dots
GPI	Glycosylphosphatidylinositol
VEGF	vascular endothelial growth factor

DMEM	Dulbecco's Modified Eagle's Medium,
FBS	Fetal bovine serum
PBS	phosphate-buffered saline
Ab	Antibody
mAb	monoclonal antibody
DMSO	Dimethyl Sulfoxide
ROI	Region on interest
RPMI	Roswell Park Memorial Institute
MVD	Microvessel density
PDX	patient-derived xenograft

1. Introduction

1.1 Challenges of diagnosis and treatment for pancreatic cancer

As one of the deadliest human malignancies, pancreatic cancer is commonly diagnosed at an advanced stage, resulting in 5-years relative survival of 9% only (Siegel et al., 2019). For pancreatic cancer, radical surgery may be the only curative treatment so far, and delineation of tumor margins is essential for radical surgery which remains challenging in practice(DeVita VT, 2005). Moreover, patients with pancreatic cancer usually bear small metastatic disease that is hardly to be detected by traditional diagnostic methods. Surgeons can only depend on visual and tactile sensation to determine the boundaries of resection along with traditional preoperative radiation imaging or magnetic resonance imaging modalities. Clinical imaging modalities have a great spatial resolution but they cannot be used intraoperatively. Intraoperative biopsies could sometimes be used for monitoring the tumor margins, however it is impractical for tumor margin delineation. Consequently, it was reported that as many as 80% of pancreatic resections are not considered radical resection due to positive surgical margin (less than 1 mm from the tumor margin), which remains a risky factor for postoperative recurrence (Markov et al., 2016; Strobel et al., 2017). Therefore, new diagnostic strategies for pancreatic cancer are urgently required.

1.2 Near-infrared fluorescent molecular imaging for pancreatic cancer

Near-infrared (NIR) fluorescent molecular imaging can overcome the above-mentioned challenges for intraoperative diagnosis of pancreatic cancer.

1.2.1. NIR fluorescent molecular imaging

Fluorescent molecular imaging has many advantages compared with traditional clinical imaging modalities. Firstly, by using targeted tracers, the detection of tumor lesions has high sensitivity and specificity. Tumor-selective molecules on the cell surface are the main targets for NIR fluorescent molecular imaging, and the targeted molecules include cell receptors and

adhesion proteins (Ogawa et al., 2009). Additionally, due to its physical properties, NIR Fluorescence allows noninvasive visualization of tumors with several millimeters in depth, while no ionizing radiation is used. (Frangioni, 2008; Mahmood and Weissleder, 2003). The advent of fluorescent molecular tomography (FMT) demonstrates the ability for quantification, and it is reported to be able to image to a depth of 10 cm (Ntziachristos, 2006). Furthermore, the currently used NIR fluorescent tracer with emission wavelengths between 700 and 2500 nm has led to a low background (auto)fluorescence (Fig.1-1) (Frangioni, 2003; Weissleder and Ntziachristos, 2003).

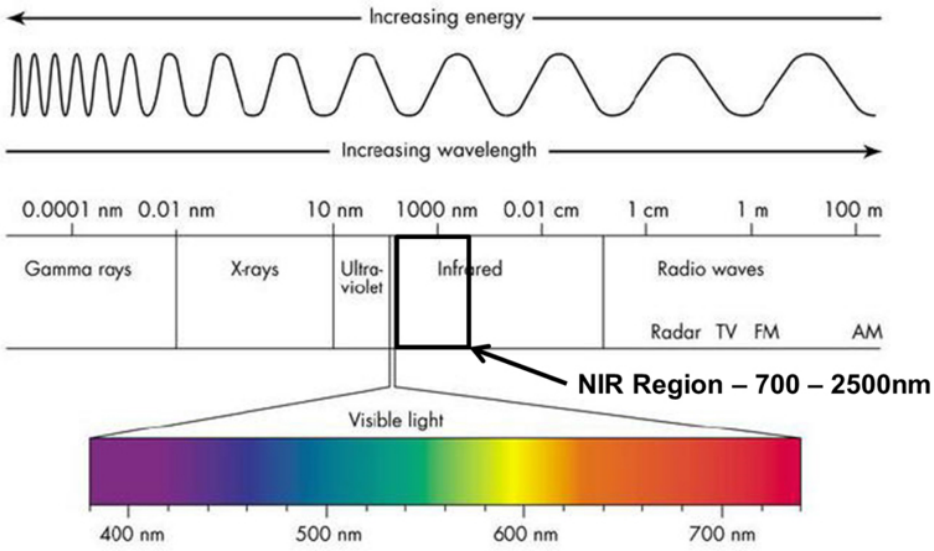

(Fig.1-1 Diagram of light spectrum, the picture was downloaded from the website below http://www.processsensors.com/appbl_II/?p=2998)

1.2.2. NIR fluorescent molecular imaging probes

Of the organic probes, there are mainly non-targeted NIR fluorescent probes and targeted NIR fluorescent probes in use.

Non-targeted organic NIR fluorescent probes

Of the non-targeted organic NIR fluorescent probes, indocyanine green (ICG) has been developed commercially for more than 50 years and widely used in clinical application.

However, ICG as a non-targeted NIR fluorescent probe yields low signal-to-noise ratio (Gioux et al., 2010). The hydrophobicity, photosensitivity and low tumor cell specificity limit the wide use of these small molecular probes in clinical cancer diagnosis and fluorescent tumor guidance in the operation, and further highlight the importance of designing and synthesizing new tumor specific NIR fluorescent probes (RP., 2002.).

Targeted organic NIR fluorescent probes

The target organic fluorescence probe is conjugating the fluorescence probe with a ligand that can bind to a specific molecule on the cell surface. The coupling fluorescent probe can be bound to and remain at the target site, while the non-binding fluorescent probe is removed in the blood circulation. As cancers have selective expression of some molecules on the cancer cell surface or in the tumor microenvironment, this method is most valuable for tumor specific imaging.

Ligands can be small molecules, peptides, proteins, and antibodies. The fluorescent groups that can be combined now include IRDye800CW, Cy5.5, etc. Although FDA has not approved these relevant probes for clinical application, relevant clinical experiments have been carried out (Whitley et al., 2016).

The IRDye800CW dye carries an NHS ester reactive group and can be conjugated with high molecular weight (45-200 kDa) proteins. The spectral properties with an absorption and emission maximum of 774 nm and 789 nm separately are comparable to FMT imager with 800 nm channel. The NIR fluorescent probe of IRDye800CW has been proven with high stability and low toxicity (Kovar et al., 2007).

Inorganic NIR fluorescent probes

Inorganic NIR fluorescent probes are mainly composed of quantum dots (QDs) (Bharali and Mousa, 2010; Nurunnabi et al., 2010) and other nanoparticles (NPs) (He et al., 2010; Wang et al., 2005). While for the non-organic probes, high cytotoxicity has limited their biological applications.

The advantages of NIR fluorescent molecular imaging

First, NIR fluorescent molecular imaging is a non-invasive optical imaging modality. NIR fluorescence can penetrate several millimeters in tissue, without ionizing radiation allowing non-invasive visualization of tumors. FMT was reported to be able to image into a depth of 10 cm (Ntziachristos, 2006). While the current predominant clinical imaging system has disadvantages of not only radioactive risks but also low specificity and sensitivity for diagnosis of malignant cancers (Fass, 2008).

Second, by using tracer targets, NIR fluorescent molecular imaging yield high sensitivity and specificity with low autofluorescence background (Frangioni, 2003; Hilderbrand and Weissleder, 2010; Pysz et al., 2010). In the "NIR window" of 650-900 nm biological tissues have low light absorption, thus deep tissue penetration and sensitive detection could be achieved based on highly fluorescent molecular probes (Mahmood and Weissleder, 2003), by which tumors and small metastases could be specifically visualized. It can be used for in vivo diagnosis, as well as for therapeutic testing. In humans, it can also not only improve the diagnosis of cancer, but also assist radical resection of malignancy, which is essential for current cancer treatment.

1.2.3 CEACAM5 is a potential target for NIR fluorescent molecular imaging

1.2.3.1 Structure of the CEACAM family

The carcinoembryonic antigen-associated cell adhesion molecule (CEACAM) gene family contains 33 genes, 22 of which are expressed (Hammarstrom, 1999). All family members have similar structural characteristics with variable and/or constant domains. This group is divided into two main groups: 1) CEACAM; 2) pregnancy-specific glycoprotein (PSG) subgroup. CEACAMs are mainly composed of seven expressed genes (Hammarstrom, 1999) (Fig.1-2).

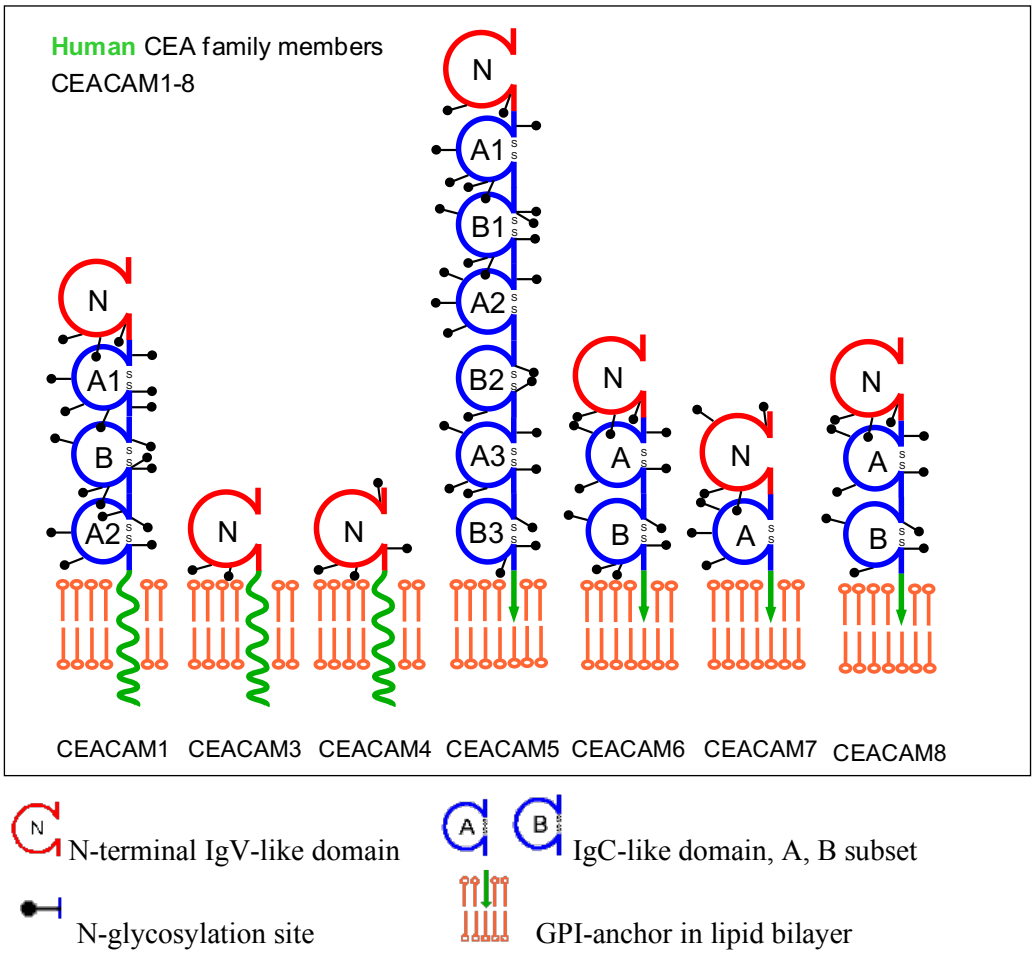

Fig.1-2: Schematic model of CEACAMs family members nomenclature (Beauchemin et al., 1999; Hammarstrom, 1999)

According to their anchoring membrane, they can be again divided into two groups: CEACAM5 (CEA), CEACAM6, CEACAM7, and CEACAM8 belong to glycophosphatidylinositol (GPI) anchor members, while CEACAM1, CEACAM3, and CEACAM4 are transmembrane members.

These membrane-bound proteins could be secreted into circulation. Of which, CEACAM5 has an important regulating influence on differentiation and proliferation of cancer cells. Overexpression of CEACAM5 may contribute to the development of many digestive or pulmonary cancers.

1.2.3.2 Expression of CEACAM5

CEACAM5, as a well-known tumor marker with a molecular weight of 180,000, is first described in human colon cancer tissue extracts by Gold and Freedman (Gold and Freedman, 1965). Its expression in the normal epithelium is very low, however, during carcinogenesis, CEACAM5 has a high expression in many epithelial originated malignancies (Hefta et al., 1998; Shively and Beatty, 1985). Adenocarcinoma of the pancreas is of no exception, where increased CEACAM5 expression has been reported (Albers et al., 1988; Allum et al., 1986; Hammarstrom, 1999; Yamaguchi et al., 1991). In addition, the protein can be secreted into the circulatory system and be measured as a serum tumor marker that reflects the disease burden.

1.2.3.3 Protein epitopes of CEACAM5

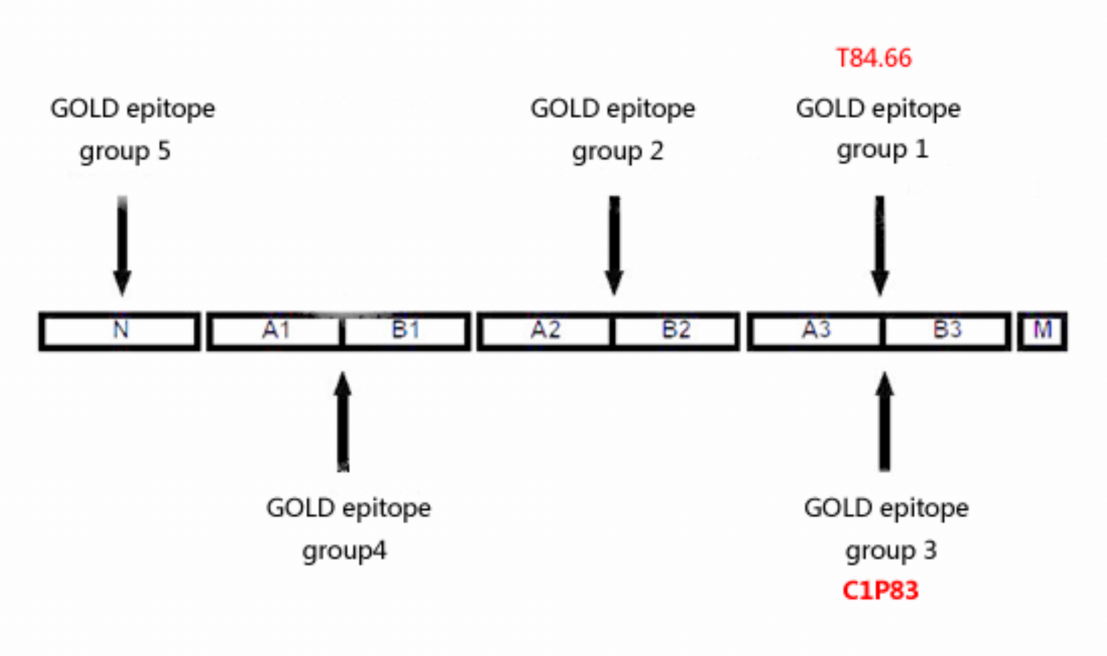

Fig.1-3 The GOLD epitope groups of CEACAM5. (Bjerner et al., 2002; Hammarstrom et al., 1989)

Human CEACAM5 is the first tumor marker subjected to epitope mapping by International Society for Cancer Developmental Biology and Medicine (ISOBM) (Hammarstrom et al., 1989). CEACAM5 consists of an N-terminal IgV-like domain (N) and six IgC-like domains (A1-3 and B1-3). It is anchored by a glycosylphosphatidylinositol to the top of epithelial cells (called C). Therefore CEACAM5 can be formulated as N-A1B1-A2B2-A3B3-C via domains (Bjerner et al., 2002; Hammarstrom et al., 1989).

According to the specificity of domain binding, five non-overlapping epitopes were divided (Fig.1-3) (Bjerner et al., 2002; Hammarstrom et al., 1989): In A3B3 domain there are GOLD epitope group 1 and 3; in A2B2 domain it is group 2; in A1B1 domain it is group 4; and in N domain binding it is group 5. However, many monoclonal antibodies against CEACAM5 were reported to have immunological cross-reactivity with NCA (CEACAM1) due to the high sequence homology in the CEACAMs subfamily (von Kleist et al., 1972) and BGP (CEACAM6) (Hinoda et al., 1988).

1.2.3.4 CEACAM5 is a promising target for molecular imaging of pancreatic cancer

Pancreatic cancer has very poor survival because its symptoms and diagnosis typically occur at an advanced stage. As CEACAM5 is selectively expressed in pancreatic cancer cells, NIR fluorescent molecular imaging targeting CEACAM5 is beneficial for diagnosis.

Some studies pointed out that circulating level of CEACAM5 in patients with pancreatic cancer increased, suggesting that serum CEACAM5 concentration can be used as a diagnostic tool and therapeutic monitoring marker. However, due to the high variability among individuals, circulating CEACAM5 concentration cannot yet yield sufficient sensitivity or specificity for diagnosis. In vivo imaging may provide a true expression of CEACAM5 thus more reliable than serum level.

CEACAM5 may be a good target for NIR fluorescent molecular imaging in vivo. Some authors reported improved pancreatic cancer fluorescence imaging by modifying monoclonal antibodies targeting CEACAM5 epitope GOLD 1 and the results showed a higher tumor-to-background ratio (Lwin et al., 2018).

1.3 Fluorescence-Guided Surgery

Based on intraoperative NIR fluorescence imaging technology, the recent fluorescence-guided surgery (FGS) has become a surgical modality. FGS can help surgeons visualize the primary tumor, all metastatic lesions and their margins during surgery by combining tumor targeting antibodies with fluorophores. And it has been shown to prolong tumor-free survival in orthotopic animal models (Hiroshima et al., 2014; Metildi et al., 2014; Metildi et al., 2013;

Uehara et al., 2015; Yano et al., 2015a; Yano et al., 2015b; Yano et al., 2016; Yano et al., 2015c).

1.4 Aim of the study

The identification of cancer cell specific and membranous antigens has laid the foundation for opening the door to molecular imaging known as a living "immunohistochemistry", which may be promising in many aspects of cancer diagnosis and treatment in the future.

So far, various imaging targets for PDAC have been explored (Li et al., 2018b; Luo et al., 2017; Neesse et al., 2013; Trajkovic-Arsic et al., 2014).

Urokinase plasminogen activator receptor (uPAR) reveals over expression on the surface of pancreatic cancer cells. Yang et al. reported a promising NIR fluorescent molecular imaging for detection of pancreatic cancer by targeting uPAR with a novel nanoparticle probe (Yang et al., 2009).

Dr. Willmann and his colleagues compared the histological and immunohistochemical analysis of VEGF receptor 2 targeted molecular images (mouse pancreas) with CD31 (vascular endothelial cell marker) and VEGF receptor 2. The results showed that the average diameter of 1.7 mm pancreatic micro tumor could be detected by ultrasound molecular imaging (Willmann et al., 2008a; Willmann et al., 2008b; Willmann et al., 2008c; Willmann et al., 2008d)

Apart from the uPAR and VEGF receptor, integrin αvβ3, claudin-4 and carbohydrate antigen 199 were also reported in application. (Li et al., 2018b; Luo et al., 2017; Neesse et al., 2013; Trajkovic-Arsic et al., 2014).

However, the above-mentioned pancreatic cancer cell antigens may not have stable expression, and there is no possibility of clinical transformation in the short term. Finding more specific and sensitive cell surface antigen of pancreatic cancer cells may be one of the breakthrough points in clinical transformation of near infrared fluorescence imaging of pancreatic cancer.

CEACAM5 seems to be an attractive target for NIR fluorescent imaging in pancreatic malignancy as it is of high expression of CEACAM5. Through targeting CEACAM5 with

epitope 1, it was reported to represent a possible strategy to improve the ability of detecting pancreatic cancer and delineating the tumor margins in the operating field (Lwin et al., 2018).

Our team had cloned a monoclonal antibody of C1P83 against CEACAM5 targeting its epitope GOLD 3 (Nap et al., 1992; Schmiegel et al., 1985). The study aims at exploring a modality of NIR fluorescent molecular imaging of pancreatic cancer targeting CEACAM5 on epitope GOLD 3, which may be expected to evolve into the application of future fluorescent surgical navigation.

2. Materials and Methods

2.1 Animals and cell sources

Four-week-old female immunodeficient C57BL/6 FoxN1^{nu} mice (Harlan) were obtained with weight from 20 g to 25 g provided by the animal center of UKSH. Animal experiments were carried out under institutional guidelines and certified by the Animal Experiment Ethics Committee of UKSH [number, V312-72241,121-33(8-1/12].

Two PDAC cell lines (PANC-1, BxPC-3) and MC38 (methycholanthrene-induced murine colon carcinoma cell line) were obtained from UKSH. The C15A3 cell line (a stable CEACAM5-expressing transfectoma from MC 38) was a gift from Dr. rer. nat. Stefanie Nittka from the University Hospital Mannheim. PANC-1 and BxPC-3 cells were cultured in RPMI 1640 medium, while MC38 and C15A3 in DMEM medium with 1 mg/ml G418 contained in the culture medium for C15A3.

2.2 Materials

2.2.1 Main Instruments

Description (Type)	Company
Beckman Coulter DU 800CW UV/Vis Spectrophotometer	Beckman Coulter, Inc.
High frequency ultrasonics (The Vevo® 770 system)	FUJIFILM VisualSonics
Flow cytometry system (BD FACSCaliburTM)	BD Biosciences, USA
Heidolph duoMax-Rotator shake (1030)	Heidolph Instruments GmbH, Schwabach
Magnetic stirrers (MR300T)	Heidolph Instruments GmbH, Schwabach
Odyssey Infrared Imaging System (2.1)	Li-COR Bioscience
Vortex (Vortex Genie2)	Scientific industries Inc., USA
Water bath (WBT12)	Reiss-Daimler Medingen
VisEn FMT 2500TM LX	VisEn™ Medical, Bedford, MA

2.2.2 Kits

Description	Company
IRDye® 800CW kit	LI-COR Biosciences, Lincoln, NE, USA
FluoroTag™ FITC Conjugation Kit	Sigma-aldrich USA
ZebaTM Desalt Spin Columns	Thermo Scientific
Purified Mouse IgG (whole molecule);	GenScript, NJ, USA
Slide-A-Lyzer™ Dialysis Cassettes (0.5-3ml/3-12ml/12-30ml)	Thermo scientific

2.2.3 Software

Description	Company
TrueQuant imaging software	PerkinElmer
The Vevo® 2100 system software	FUJIFILM VisualSonics
ABI Prism 7700 SDS software	Applied Biosystems)
Windows XP SP2	Microsoft Inc.
SDS 2.1 software	Applied Biosystems
SPSS windows 22.0	SPSS Inc.
GraphPad Prism 6	GraphPad Software Inc.

2.3 Methods

2.3.1 Production and purification of the anti-CEACAM5 monoclonal antibody: C1P83

C1P83 was provided by Prof. H. Kalthoff (Christian Albrechts University; Kiel, Germany). The production technique was described previously(Nap et al., 1992; Schmiegel et al., 1985). The specificity and affinity of C1P83 against CEACAM5 (epitope GOLD 3) have been validated(Nap et al., 1992).

2.3.2 Conjugation of C1P83 and mouse IgG (control) with IRDye800CW.

The protocol followed is according the manufactureres instructions using the protein labelling kit for IRD800CW. The main steps are listed below.

2.3.2.1 Preparation of Protein Solution for Conjugation

100 µg of protein at a concentration of 1 (± 0.1) mg / mL was prepared in phosphate buffer (pH 8.5). Before reacting with IRDdye 800CW, cool / heat the protein to 20-25ºC.

2.3.2.2 Protein Labeling Reaction

Mix the appropriate amount of IRDdye800CW with 100 μg protein according to the Figure 2-1. React for 2 hours at 20℃ and protect the vial from light.

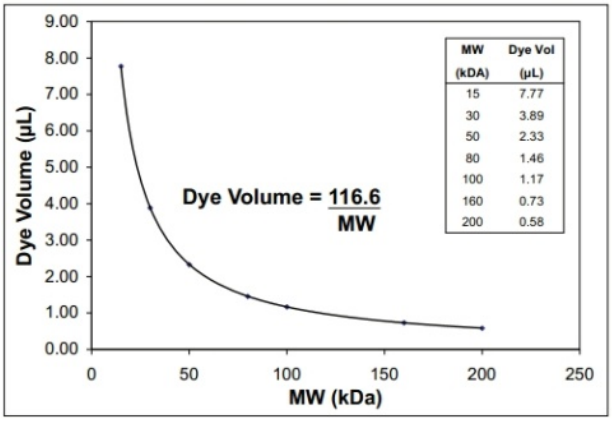

Fig.2-1 IRDdye800CW volume and the molecular weight of the protein

2.3.2.3 Conjugates of C1P83-IRDye 800CW and IgG-IRDye 800CW were purified by dialysis.

Conjugates of C1P83-IRDye 800CW and IgG-IRDye 800CW were purified by the Zebra Desalting Spin Columns and the kit of Slide-A-Lyzer™ Dialysis Cassettes (0.5-3ml/3-12ml/12-30ml).

2.3.2.4 Calculation of Dye/Protein Ratio and Protein Concentration

Measure the absorbance of the conjugate at 280 nm and 689 nm (A280 and A780). Then calculate the dye/protein ratio using the following formula:

$$D/P = \left[\frac{A_{780}}{\varepsilon_{Dye}}\right] \div \left[\frac{A_{280} - (0.03 \times A_{780})}{\varepsilon_{Protein}}\right]$$

Calculate the final protein concentration using the following formula:

$$\text{Protein conc. (mg/mL)} = \frac{A_{280} - (0.03 \times A_{780})}{\varepsilon_{Protein}} \times MW_{Protein} \times \text{dilution factor}$$

εDye is 270,000 M^{-1} cm^{-1} and εProtein is 203,000 M^{-1} cm^{-1} (for a typical IgG) in a 1: 1 mixture of PBS: methanol.

2.3.3 FACS analysis for CEACAM5

2.3.3.1 FITC labelling of antibody of C1P83 and IgG

The protocol followed is according the manufacturers instructions using the Fluortag FITC conjugation kit. The main steps are listed below.

Antibody preparation: Prepare 1 ml antibody solution with 5.0 mg / ml in 0.1 M bicarbonate buffer (pH 9.0). Add 0.2 ml (1.0 mg) of the antibody solution to each reaction vessel labeled "5: 1", "10: 1", or "20: 1".

FITC preparation: Redissolve a bottle of FITC (F7250) in 2 ml of 0.1 M carbonate bicarbonate buffer, and spin until all FITC is dissolved. Label the vial with "20: 1 FITC". The "20: 1 FITC" solution is also used to make "5: 1" and "10: 1" solutions.

Labelling: Add 50 ml of the appropriate FITC dilution to the corresponding labeled reaction vessel with stirring without light.

Dialysis: Labeled proteins were isolated by dialysis.

Calculating: Based on the absorbance values of the conjugate samples (A280 and A495), the protein concentration and F/P of the fluorescein-antibody conjugate is calculated according to the following formula:

$$\text{Molar F/P} = \frac{2.77 \times A_{495}}{A_{280} - (0.35 \times A_{495})} \text{ (For FITC-IgG conjugates only)} \qquad \text{IgG (mg/ml)} = \frac{A_{280} - (0.35 \times A_{495})}{1.4}$$

2.3.3.2 FACS for CEACAM5 quantification analysis in different cell lines

1) Sample preparation: The cells were centrifuged at 500 × g for 5 minutes and washed three times in an isotonic PBS buffer. Adherent cell lines Pretreatment with 0.5 mM EDTA may be required to facilitate removal from their substrates.

2) Harvest cells and Fc block cells with blocking IgG (1 µg IgG / 10^6 cells) for 15 minutes at room temperature.

3) Add conjugated antibody (10 µl / 10^6 cells or a previously titrated amount).

4) Remove all unbound antibodies by washing and centrifuge the suspended cells at 300 g for 5 minutes and decant the buffer. Resuspend the cells by adding 2 ml flow cytometry staining buffer. Repeat the washing process twice.

5) Resuspend the cells in 200-400 µl staining buffer for the final flow cytometric analysis.

2.3.4 Immunostaining for CEACAM5 location in BxPC-3 cell line

The monoclonal antibody C1P83 was used which recognizes the epitope GOLD 3 of CEACAM5. And IgG was also used as a control. In the control group, 1st Ab: ms IgG, 2nd Ab: anti-ms IgG-HRP; in C1P83 group, 1st Ab: C1P83, 2nd Ab: anti-ms IgG-HRP. Visualization was carried out with a peroxidase – diaminobenzidine kit (Dako)

2.3.5 In vitro binding experiments

For affinity measurements, 100,000 BxPC-3 cells / well were seeded into 6-well plates and allowed to adhere overnight. The next day, the medium was aspirated, the cells were blocked with 4% skim milk powder in PBS, and the cells were incubated with 2 ug of IRDye800CW-labeled C1P83 in 2% skim milk powder in PBS at 4 ° C for 2 h or 24 h. dark. Cells were washed 3 times with PBS, and fluorescence was measured and quantified using a Li-COR Odyssey infrared imaging system (λEx = 785 nm; λEm = 800 nm).

2.3.6. In vivo experiments

2.3.6.1. Animal tumor model

2.3.6.1.1. Subcutaneous tumor model

The subcutaneous tumor model has CEACAM5-positive tumors (C15A3, 1×10^6 cells) in the left abdomen and CEACAM5-negative tumors (MC38, 1×10^6 cells) in the right abdomen in the Four-week-old immunodeficient C57BL/6 FoxN1^{nu} mice (Harlan), so each mouse can be used as its own control. They were allowed to grow for 10 to 14 days, and imaging was started when significant tumors appeared.

2.3.6.1.2. Orthotopic tumor model

The aesthesis was performed by 80 mg / kg ketamine (Aveco Co., Inc.) and 10 mg / kg xylazine (Rugby Laboratories, Inc.). A small (1 cm) lateral subcostal laparotomy was performed. One million CEACAM5 positive BxPC3 cells were orthotopically injected under the capsule of the pancreas in the Four-week-old immunodeficient C57BL/6 FoxN1^{nu} mice (Harlan). The tumor growth was monitored by ultrasound and the tumors were able to grow 28

days before imaging. NIR fluorescence was visualized at various times with an FMT2500 imager (λEx = 779 nm; λEm = 795 nm). Mouse IgG-IRDye800CW conjugates were injected as controls.

2.3.6.2. In vivo high-resolution sonography

Tumor volume was assessed by Vevo 770 small animal micro-imaging system (VisualSonics, Toronto, Ontario, Canada) using the Visual Sonics image analysis software package to define a three-dimensional region of interest. Select the tumor area of interest by acquiring ultrasound images that displays the maximum lateral diameter of the tumor for analysis.

2.3.6.3. In vivo high-resolution MRI

MRI imaging was performed on xenografted mice under general anesthesia with isoflurane by a 7-T MRI for small animal imaging (Cliniscan, Bruker Biospin GmbH, Ettlingen, Germany) with protocols as described in the literature (Will et al., 2016).

2.3.6.4. NIR fluorescent molecular imaging in vivo and Image ex vivo

Images were taken daily by FMT2500LX until 7 days after the injection. The same size of the region of interest (ROI) was used for the comparison between the two groups. In addition, an ROI of the same size was generated in a representative region without tumor tissue in order to determine the background fluorescence.

2.3.7. Histological Study

Histological study was composed of Hematoxylin and Eosin Staining, Masson's Trichrome Staining and Microvessel density detection for tumor tissues.

Masson's Trichrome Staining was used to detect collagen fibers in tissues on formalin-fixed sections embedded in paraffin. The collagen fibers are colored blue and the cores are colored black and the background is colored red.

Microvessel density (MVD) was assessed by immunohistochemical staining with anti-CD31 antibodies. MVD was determined by identifying the three most intense neovascular

regions of each sample and counting at low magnifications (100x magnification). Record average number of vessels in three selected areas

2.3.8 Statistical analysis

Statistical analysis was carried out by IBM SPSS Statistics version 23.0 and GraphPad Prism7.0. Mann-Whitney U test or one-way ANOVA was used with one variable involved. When there were two variables, two-way ANOVA was used for analysis. P values < 0.05 was were considered to be statistically significant. Spearman rank correlation coefficient was chosen for correlation analysis ($\alpha = 0.05$).

3. Results

3.1 CEACAM5 qualitative and quantitative analysis in different cell lines

3.1.1 Human BxPC-3 pancreatic cancer cell line is CEACAM5 positive by FACS analysis and immunocytochemistry

To determine the expression of CEA on pancreatic tumor cell lines for the purposes of establishing an orthotopic in-vivo tumor model for testing the antibody, the C1P83 antibody was incubated with BxPC3 and Panc1 cell lines and detected using a secondary antibody conjugate to FITC and analyzed by flow cytometry.

FACS analysis

FACS analysis indicated that BxPC-3 is a CEACAM5-positive cell line (Fig.3-1B) (Fig.3-1A)

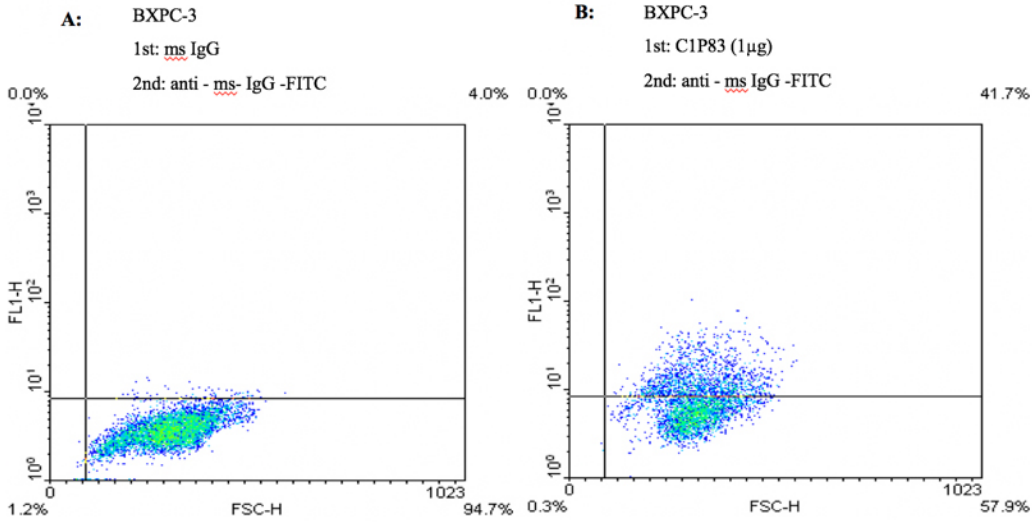

Fig.3-1 FACS analysis showed that human BxPC-3 pancreatic cancer cell line is CEACAM5 positive.

Further immunocytochemistry showed that CEACAM5 is expressed on the membrane of BxPC-3 pancreatic cancer cells (Fig.3-2B).

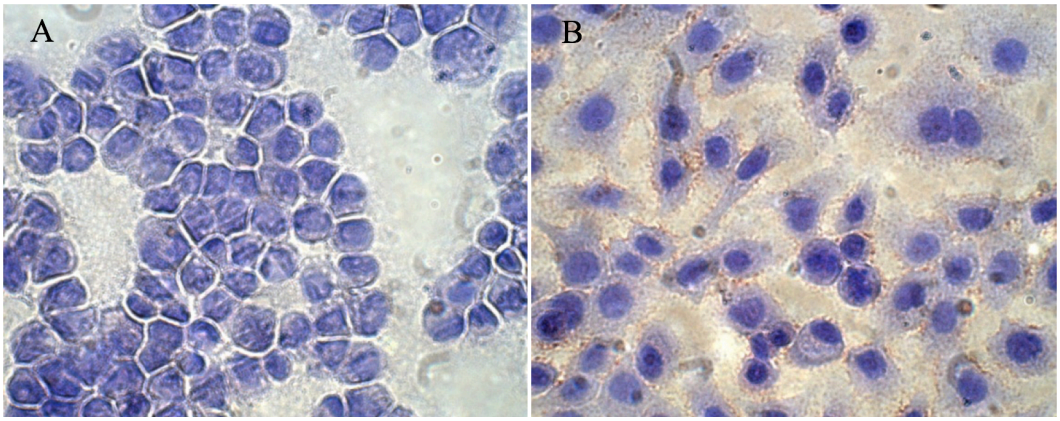

Fig.3-2 Immunocytochemistry showed CEACAM5 is expressed on the membrane of BxPC-3 pancreatic cancer cells (B). A(control): 1st Ab: ms IgG, 2nd Ab: anti-ms, IgG-HRP. B: 1st Ab: C1P83, 2nd Ab: anti-ms IgG-HRP.

3.1.2. Human PANC-1 pancreatic cancer cell line is CEACAM5 negative

FACS analysis showed the PANC-1 cell line is a CEACAM5 negative cell line.

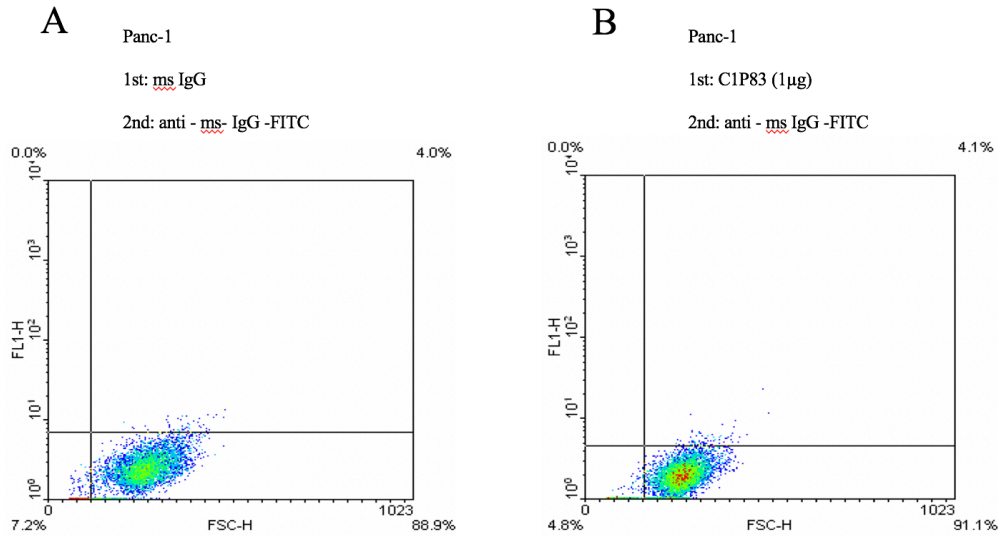

Fig.3-3. FACS analysis showed that PANC-1 pancreatic cancer cell line is CEACAM5-negative.

3.1.3. Murine CEACAM5^{+} C15A3 cell line is CEACAM5 positive

To establish a positive control for determining CEA expression in-vitro and in-vivo, the CEACAM5^{+} C15A3 murine colon carcinoma cell line (stably transfected with human

CEACAM5) was utilized. Cells were incubated with the primary antibody and primary antibody binding was detected by a secondary antibody conjugated to FITC. C15A3 cell line was confirmed to be CEACAM5 positive by FACS analysis. (Fig.3-4A, Fig.3-4B)

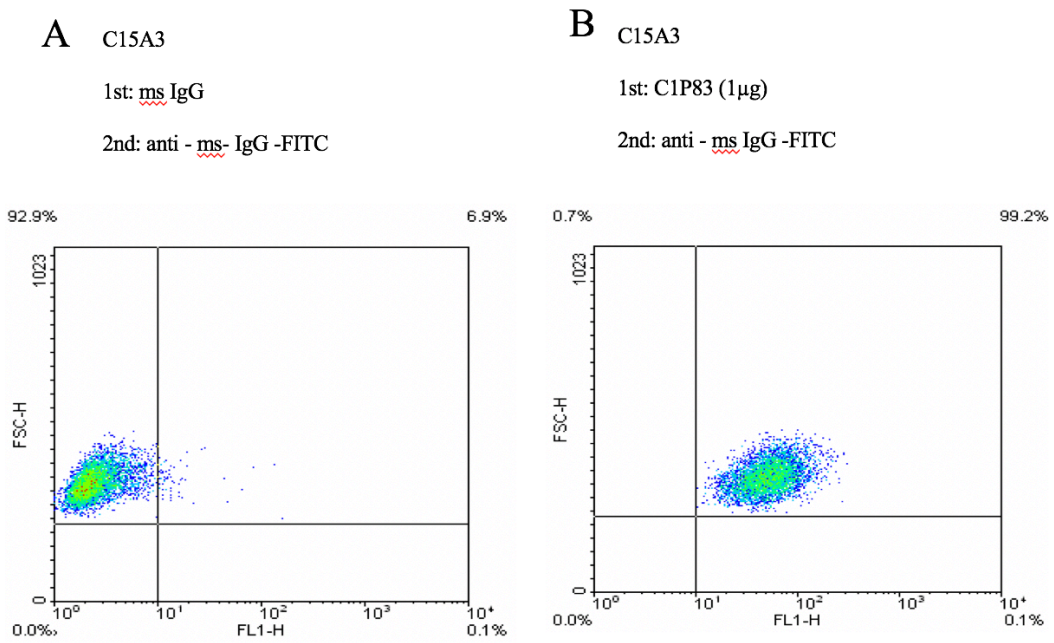

Fig.3-4 FACS analysis showed that C15A3 cell line (stably transfected with human CEACAM5) is CEACAM5 positive.

3.1.4. Murine CEACAM5⁻ MC38 cell line is CEACAM5 negative

FACS analysis showed that that MC38 murine colon carcinoma cell line is CEACAM5-negative. (Fig.3-5A, Fig.3-5B)

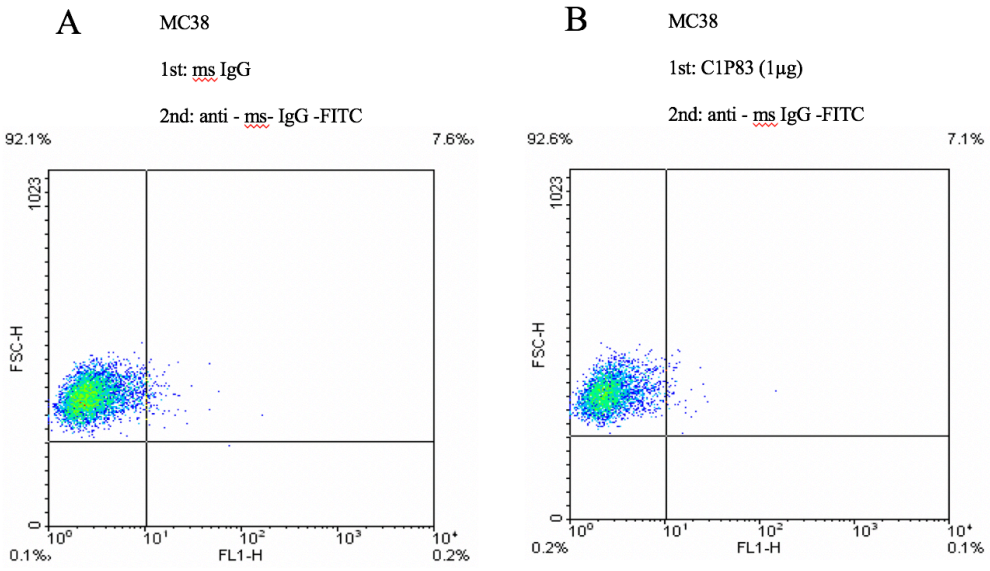

Fig.3-5 Negative expression of CEACAM5 in MC38 cell line by FACS.

3.2 CEACAM5 targeted NIR fluorescent imaging: in vitro experiment

3.2.1 C1P83-IRDye800CW specifically bind to CEACAM5 positive BxPC-3 cells

For in-vivo detection of antibody binding, it is advantageous to use near-infrared fluorochromes since the emission wavelength is minimally absorbed by bodily fluids and tissue. However, conjugation of the fluorochrome to the antibody may alter binding of the antibody to its target. The antibody C1P83 was conjugated to IRDye800CW on lysine residues. To ensure that the conjugated antibody maintained binding activity to the target epitope, in-vitro binding experiments were performed. Li-COR Odyssey infrared imager indicated that the conjugates of C1P83-IRDye800CW could specifically bind CEACAM5 positive BxPC-3 pancreatic cancer cells; CEACAM5 positive BxPC-3 pancreatic cancer cells had significantly higher fluorescence (pmol) than CEACAM5-negative PANC-1 pancreatic cancer cells (P <0.05). (Fig.3-6) (After the conjugation with IRD800CW for C1P83, the Dye/Protein Ratio was 2, and the concentration was 0.5 ug/ul)

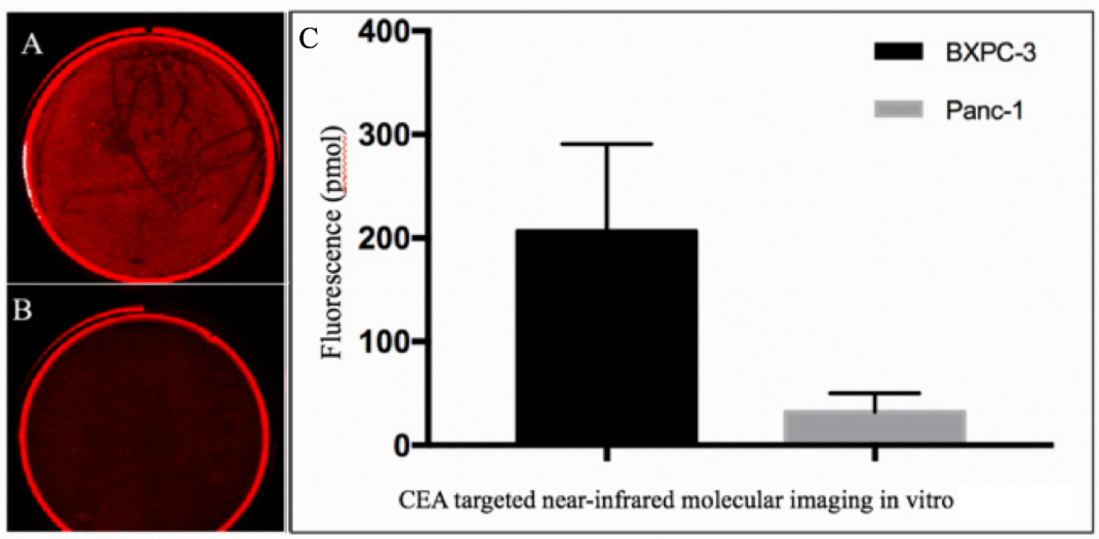

Fig.3-6 CEACAM5 targeted NIR fluorescent molecular imaging in vitro in BxPC-3 and PANC-1 cancer cells. A: C1P83-IRDye800CW was added to BxPC-3 cell culture medium for 2 hours (six-well plate); B: C1P83-IRDye800CW was added to PANC-1 cell culture medium for 2 hours (six-well plate); C: Comparison of fluorescence (pmol) 2 hours after the addition of C1P83-IRDye800CW in vitro between BxPC-3 and PANC-1 cell lines in six-well plate (P <0.01).

3.3 CEACAM5 targeted NIR fluorescence molecular imaging in vivo: subcutaneous tumor model

To establish specificity in detection of CEA expressing tumors in-vivo using the C1P83-IRD800CW, an in-vivo experiment was performed in mice harboring CEA non-expressing and CEA expressing tumors. The CEA negative cell line MC38 was inoculated subcutaneously on one flank of the mice and the CEA expressing cell line C1P83 on the opposite flank. Of note was the rapid growth of MC38 in contrast to C15A3 tumors which remained small. Despite the difference in size of the tumor, the CEA expressing tumor could be clearly detected.

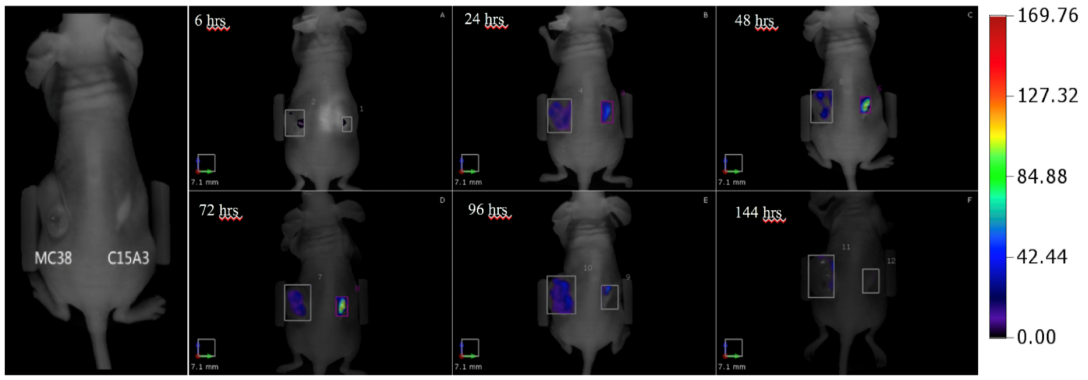

Fig.3-7 CEACAM5 targeted NIR fluorescent molecular imaging of subcutaneous tumor. MC38 (left): CEACAM5-, C15A3 (right): CEACAM5 +

As shown in Fig.3-7, after injection of 25ug IRDye800CW labelled antibody into the mice by the tail vein (n = 5), the NIR fluorescence imaging model of subcutaneous tumors showed that the fluorescence intensity (nM) of CEACAM5 positive C15A3 subcutaneous tumors were significantly higher than that of CEACAM5 negative MC38 subcutaneous tumors, and the fluorescence intensity peaked around 48 hours after C1P83-IRDye80CW injection (Fig. 3-8).

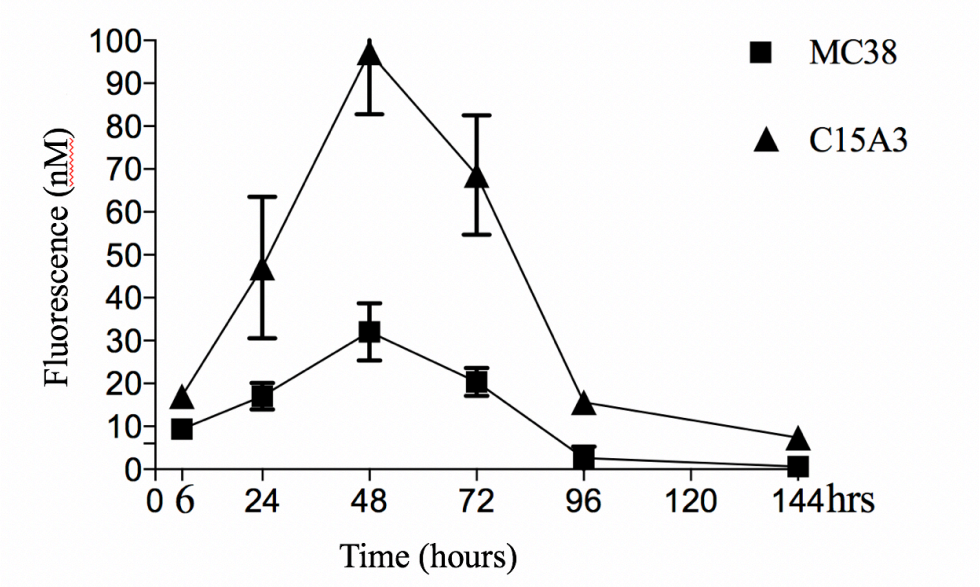

Fig.3-8 NIR fluorescence intensity and time curve in the subcutaneous tumor model (MC38 vs C15A3).

3.4 CEACAM5 targeted NIR fluorescent molecular imaging in vivo: orthotopic pancreatic tumor model

To test the sensitivity of the antibody in a more clinically relevant mouse model, mice were orthotopically inoculated with the BxPC3 cell line. Two weeks after orthotopic inoculation, tumors can be detected by 3-D ultrasound in each mouse, with the diameter 3-5 mm. The NIR fluorescent imaging was performed about four weeks after orthotopic inoculation. For orthotopic tumor imaging, after the conjugation with IRD800CW for C1P83, the Dye/Protein Ratio was 2, and the concentration was 0.5 ug/ul; mouse IgG Dye/Protein Ratio was 1.1, and the concentration was 1.2 ug/ul.

3.4.1. Dosage with 25 ug C1P83 or IgG injected.

(1) IgG control group:

As shown in Fig.3-9: After the injection of 25ug IRD800CW labelled IgG, most of the NIR fluorescence (nM) stayed in the liver, and the tumor-specific fluorescence (nM) at the tumor site was very weak. (n = 3)

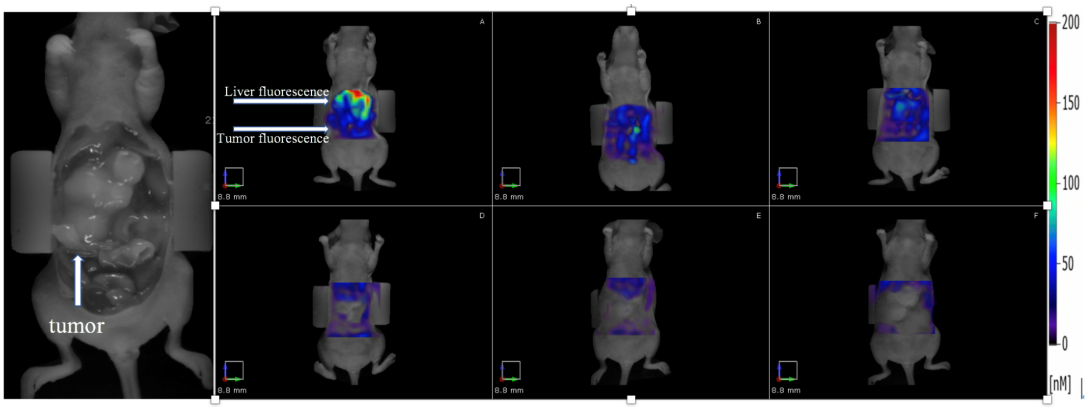

Fig.3-9 NIR fluorescent imaging of pancreatic orthotopic tumor (25 ug IgG, control group)

(2) C1P83 group:

As shown in Fig.3-10, the tumor-specific NIR fluorescence signal was significantly increased compared with the control group, and the fluorescence intensity peaked after 48-72 hours, and the fluorescence can be maintained for nearly one week. (n = 5)

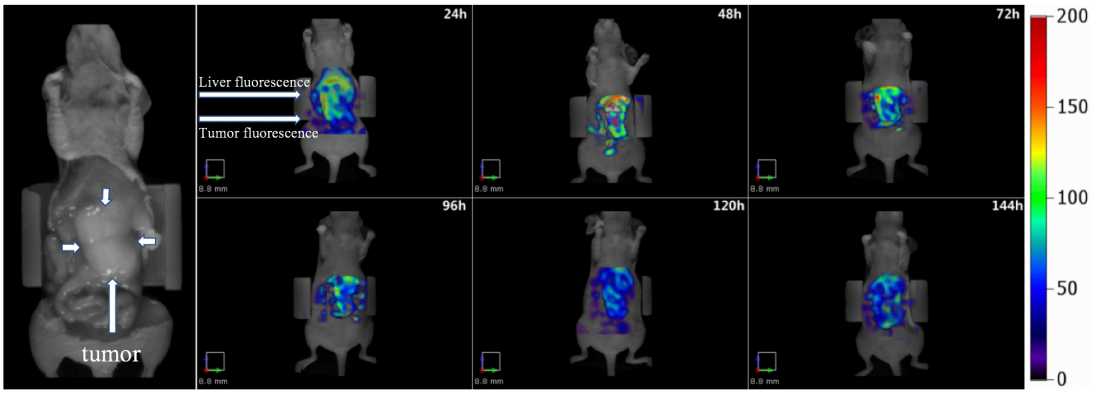

Fig.3-10 NIR fluorescence imaging of pancreatic orthotopic tumor (25 ug C1P83 group)

(3) Time and fluorescence

The results suggested that the NIR fluorescence in the C1P83 group was higher than that of the IgG control group ($P < 0.05$), and the fluorescence started to fade after 48-72 hours ($P < 0.05$). (Fig.3-11)

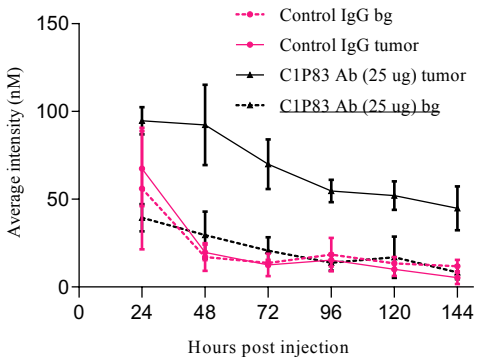

Fig.3-11 Time-fluorescence curve. (bg: background) (n=x Control IgG bg, n=y Control IgG tumor, n=z C1P83 tumor, n=xx C1p83 Ab bg)

(4) Tumor-to-background ratio:

The results suggested that the NIR fluorescent tumor-to-background ratio (TBR) of the C1P83 group is significantly higher compared with that of the IgG group ($P < 0.05$), and the TBR does not increase significantly with time (Fig. 3-12) ($P = 0.295$).

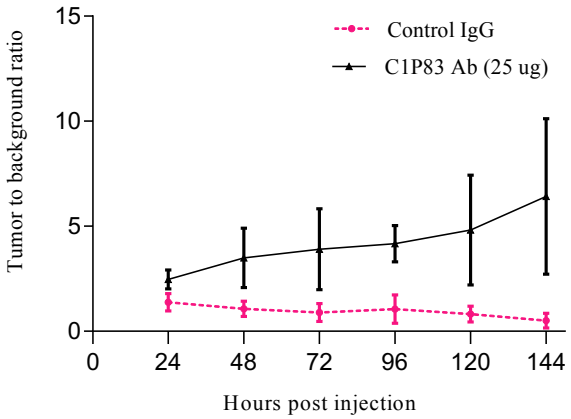

Fig.3-12 NIR fluorescent tumor-to-background ratio (25ug dosage group)

(5) Ex vivo imaging, biodistribution and histological study

Ex vivo NIR fluorescent imaging (144 hours after injection of IRD800CW labelled antibody) showed that the NIR fluorescent (nM) of the tumor tissue was significantly higher than that of liver, spleen, and kidney (see Fig.3-13, Fig.3-14). Tumor weight-fluorescence curve showed that there was a correlation between the tumor weight (ex vivo) and the fluorescence (pmol) ($R^2 = 0.8017$, $P < 0.0001$) (Fig.3-15).

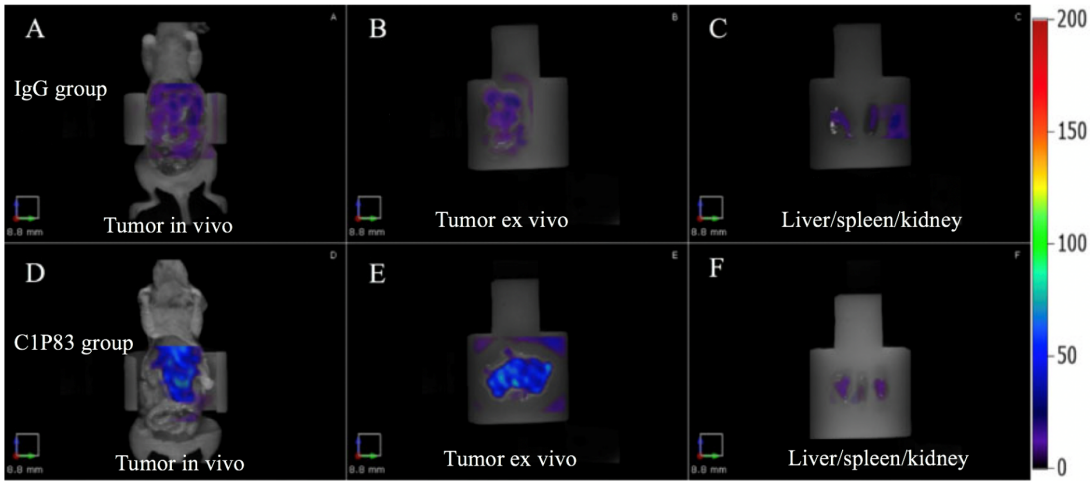

Fig.3-13 Biodistribution of NIR fluorescence ex vivo. IgG control group: (A): In vivo NIR fluorescent molecular imaging of tumors in the IgG control group;

(B): Ex vivo NIR fluorescent molecular imaging of tumors in the IgG group;

(C): Ex vivo NIR fluorescent molecular imaging of liver, spleen, and kidney in the IgG group;

(D): In vivo NIR fluorescent molecular imaging of tumors in the C1P83 group;

(E): Ex vivo NIR fluorescent molecular imaging of tumors in the C1P83 group;

(F): Ex vivo NIR fluorescent molecular imaging of liver, spleen, and kidney in the C1P83 group;

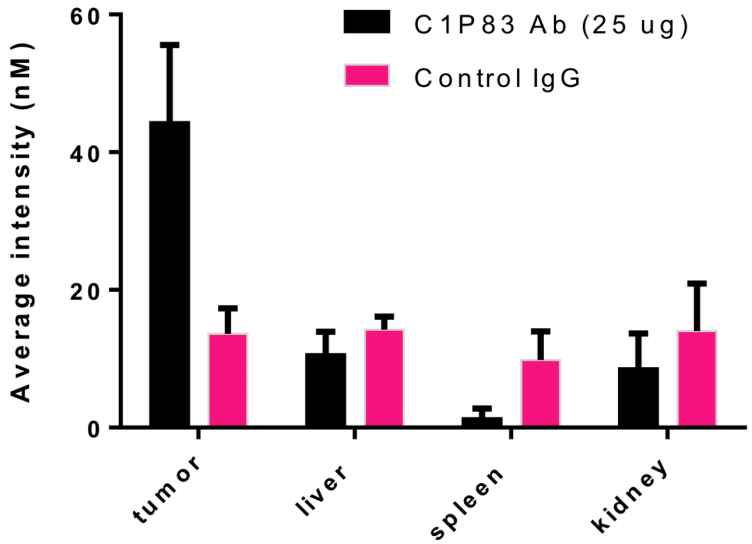

Fig.3-14 Biodistribution of fluorescence in the C1P83 group and the IgG control group ($P < 0.05$).

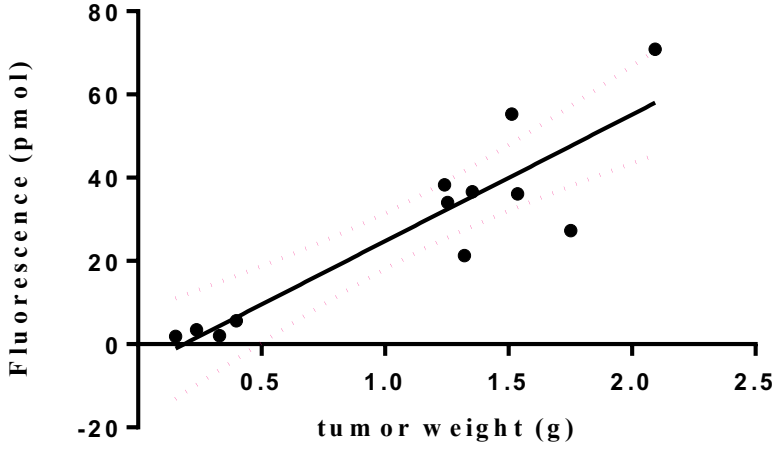

Fig.3-15 Tumor weight was correlated with the fluorescence (R^2 = 0.8017, P <0.0001, Equation: Y = 30.40 * X-5.656) (25 ug group)

As shown in Fig.3-16, the tumors were confirmed ex vivo by H-E staining.

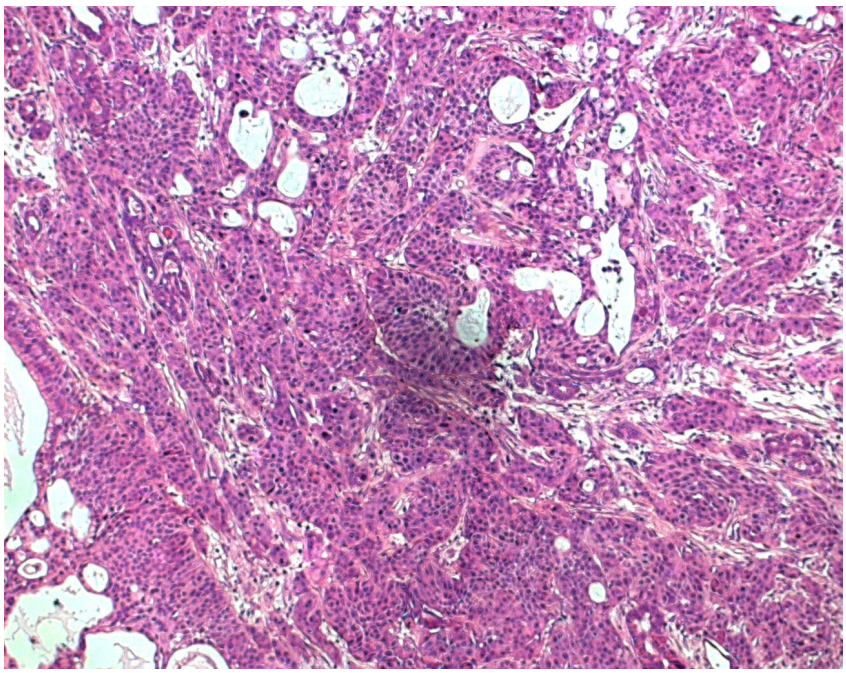

Fig.3-16 H-E staining of pancreatic cancer tumor.

3.4.2. dosage with 100 ug C1P83 or IgG injected:

To determine if sensitivity of tumor detection could be increased with higher doses of the antibody, the TBR was determined using 100ug of antibody in mice harboring BxPC3 tumors.

(1) 100 ug IgG control group

As shown in Fig.3-17: Most of the NIR fluorescence in the 100 ug IgG control group retained in the liver, and the tumor-specific fluorescence at the tumor site was very weak but detectable. (n = 3)

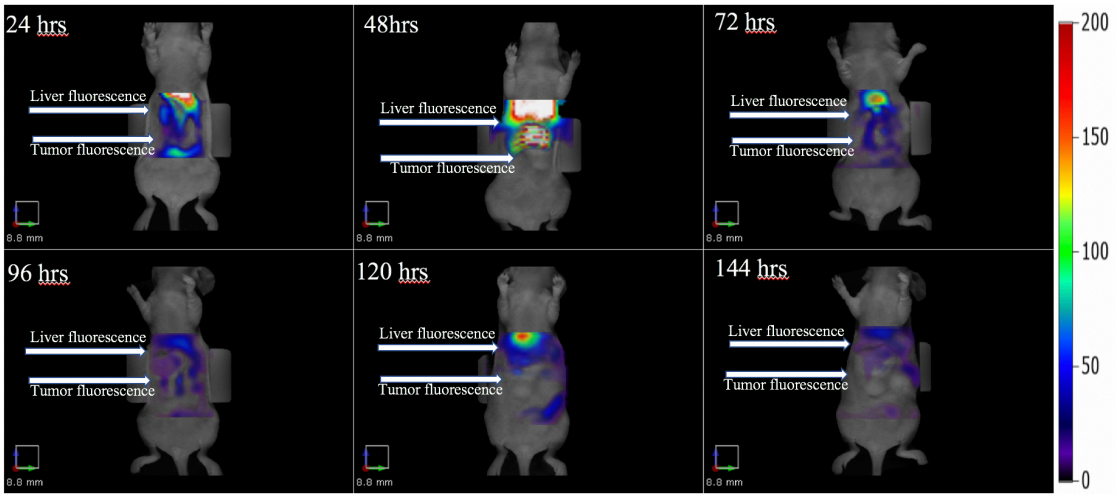

Fig.3-17 NIR fluorescent imaging of orthotopic pancreatic tumors (100 ug IgG control group)

(2) 100 ug C1P83 group

As shown in Fig.3-18, the tumor-specific NIR fluorescence was significantly increased in 100 ug C1P83 group, and the tumor fluorescence peaked after 48-72 hours; and the fluorescence can be maintained for nearly one week. (n = 5)

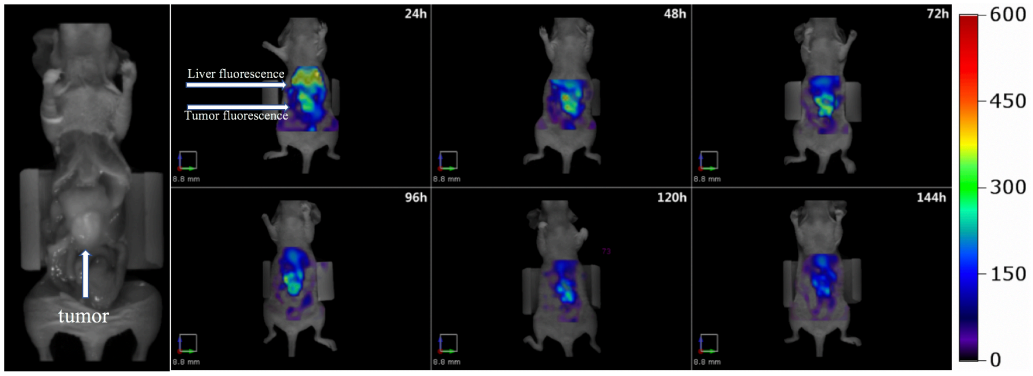

Fig.3-18 NIR fluorescence imaging model of pancreatic orthotopic tumor (100 ug C1P83 group).

(3) Time and fluorescence

The results suggested that the NIR fluorescence (nM) of the tumor in the 100ug C1P83 group was significantly higher compared with that in the 25ug C1P83 group ($P < 0.05$). The fluorescence was time-dependent which started to fade after 48-72 hours ($P < 0.05$). (Fig.3-19)

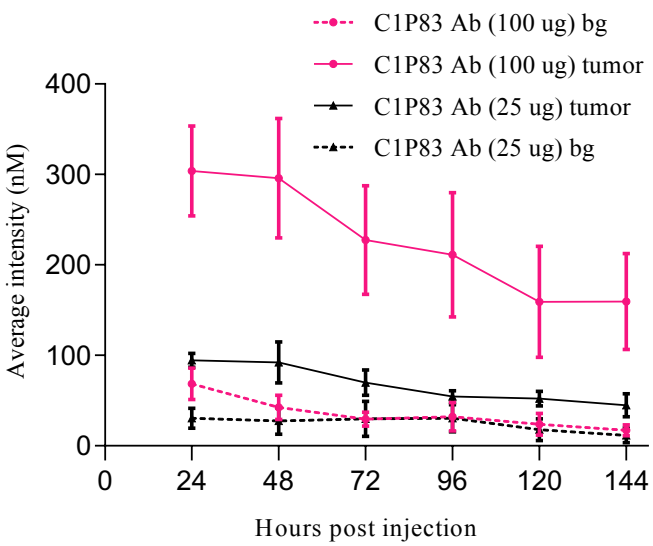

Fig.3-19 Time-fluorescence curve.

(4) Tumor-to-background ratio:

The results suggested that the TBR of the 100ug C1P83 group was higher than that of the 25ug C1P83 group, but the difference between the two groups did not reach a statistically significant level (P = 0.07). (Fig.3-20)

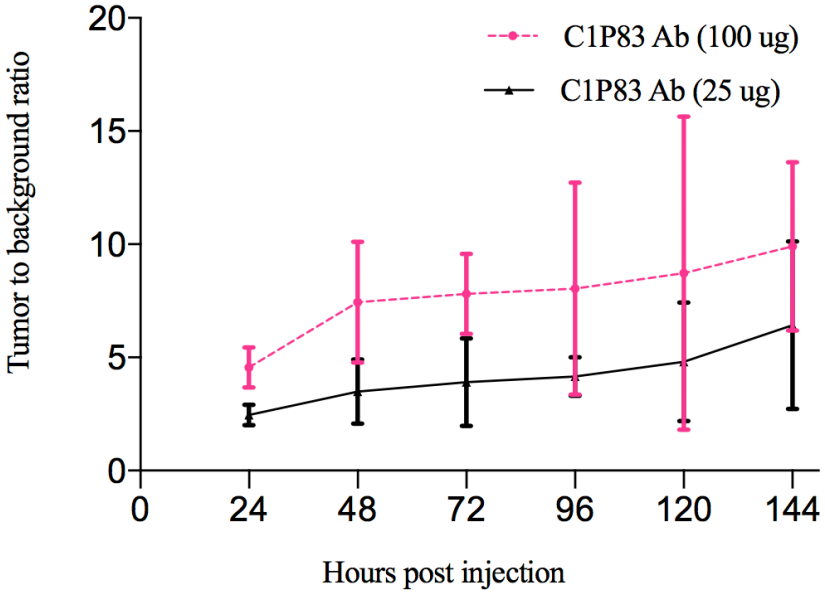

Fig.3-20 NIR fluorescent tumor-to-background ratio (TBR).

(5) Overall correlation between FMT and MRI

MRI of orthotopic pancreatic tumors (n = 9):

After the pancreatic orthotopic tumor model had been successfully established, 7-T MRI was performed for imaging of the tumors in mice, and the tumor volume was calculated with the respective software of each modality. As shown in Fig.3-21, 7-T MRI could perform sagittal, coronal, and cross-sectional imaging of pancreatic orthotopic tumors.

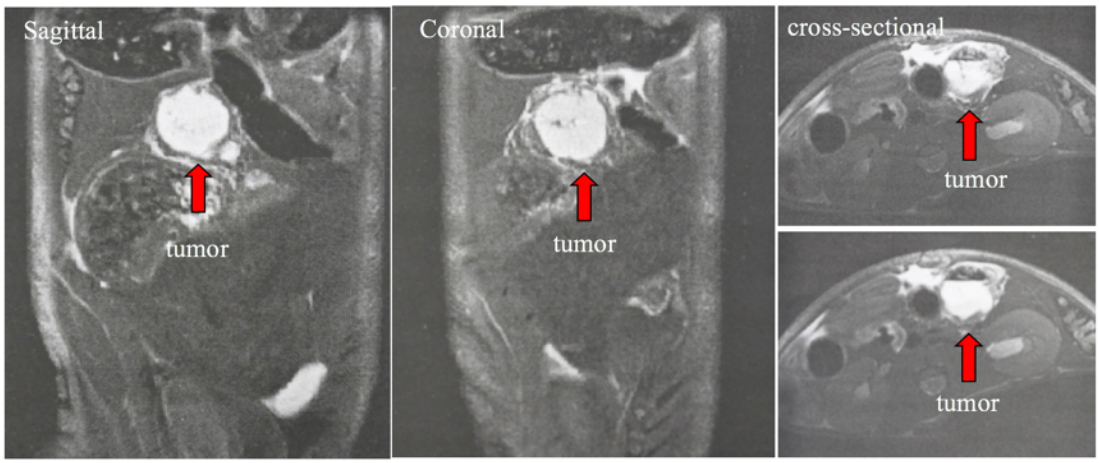

Fig.3-21 Magnetic resonance imaging of pancreatic orthotopic tumors

Relationship between pancreatic tumor volume and NIR fluorescence (n = 9):

Each mouse was injected with 100 ug of C1P83-IRDye800 conjugate in the tail vein. After 72 hours, NIR fluorescent molecular imaging was performed with a FMT2500 imager, and then 7-T MRI was used to perform magnetic resonance examination and calculation of tumors volume (mm^3). As shown in Fig.3-22 and Fig.3-23, the NIR fluorescence (pmol) of the pancreatic orthotopic tumor and the magnetic resonance tumor volume (mm^3) showed a good correlation (Pearson r = 0.9188, 95 % confidence interval : 0.6531-0.9831, R^2 = 0.8441, P = 0.0005).

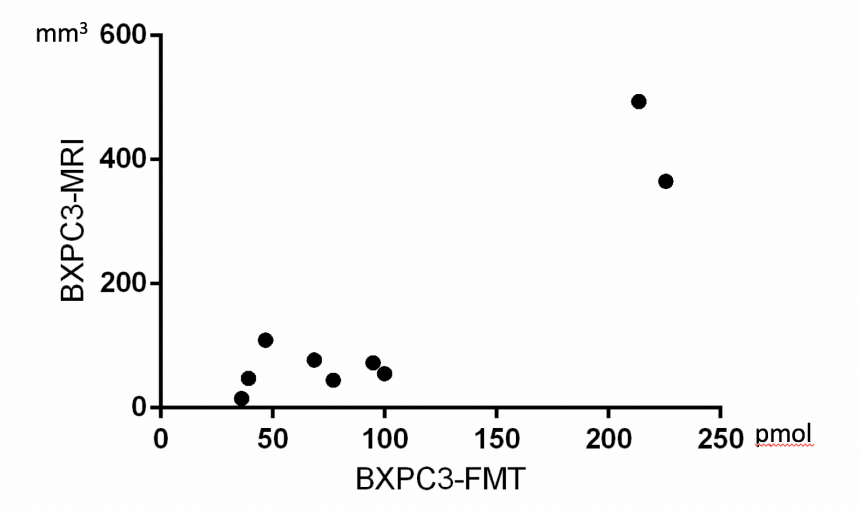

Fig.3-22 Correlation between NIR fluorescence of pancreatic orthotopic tumors and magnetic resonance tumor volume (Pearson r = 0.9188, 95% confidence interval: 0.6531-0.9831, R^2 = 0.8441, P = 0.0005, X-Y pairs = 9)

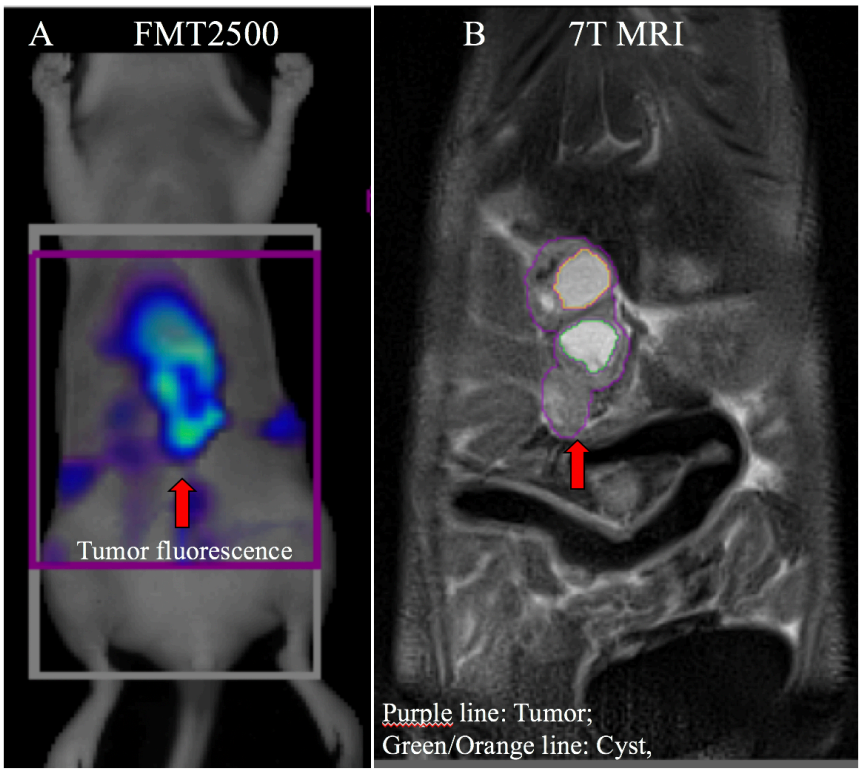

Fig.3-23 NIR fluorescent molecular imaging and magnetic resonance imaging of pancreatic orthotopic tumors (A: FMT2500 NIR fluorescent molecular imaging of pancreatic tumor in vivo; B: 7T MRI of pancreatic orthotopic tumor)

(6) Ex vivo imaging, biodistribution and histological study

Ex vivo NIR *fluorescent imaging and biological distribution of fluorescence (nM):*

The ex vivo NIR fluorescent imaging showed that the fluorescence (nM) of the tumor in the 100 ug C1P83 group was significantly higher than that of the liver, spleen, and kidney (see Fig. 3-24, Fig. 3-25).

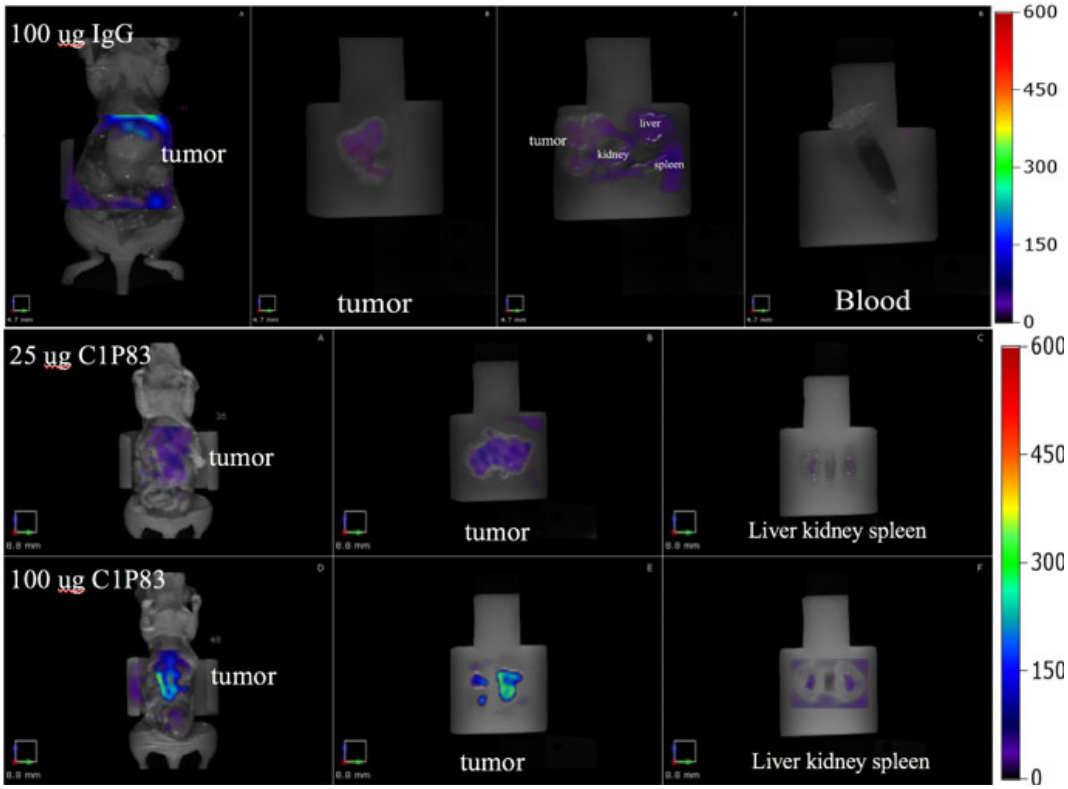

Fig.3-24 NIR fluorescent imaging of pancreatic orthotopic tumors and biological distribution of fluorescence.

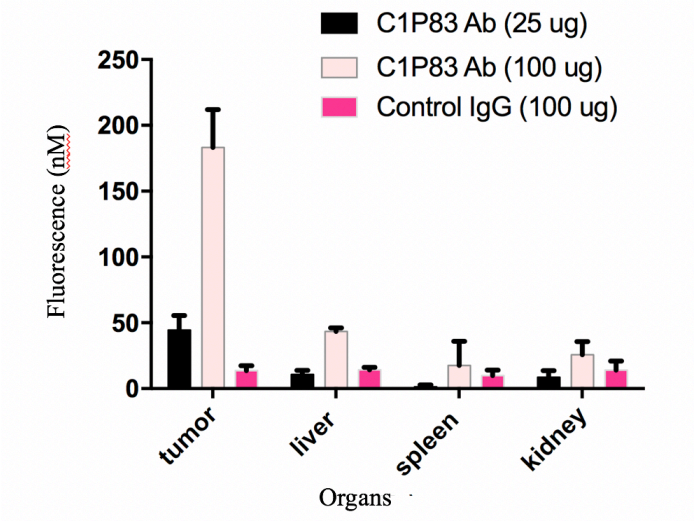

Fig.3-25 Ex vivo NIR imaging and biological distribution of fluorescence.

Tumor weight and fluorescence:

As shown in Fig.3-26, the tumor weight (g) was correlated with the NIR fluorescence (pmol) (R^2 = 0.7722, P = 0.0041).

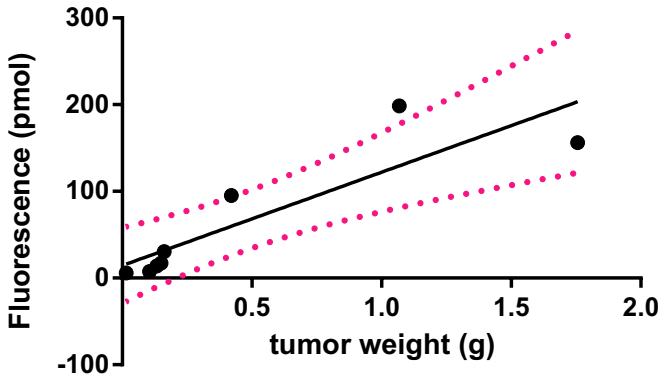

Fig.3-26 Correlation between pancreatic orthotopic tumor weight and NIR fluorescence (100 ug C1P83 group) (R^2 = 0.7722, P = 0.0041, Equation: Y = 107.6 * X + 14.46)

Biological distribution ex vivo NIR fluorescence and time:

The samples at 6/24/48 hours were 3 cases each. After injection of 100 ug IRD800CW labelled C1P83, ex vivo NIR fluorescent imaging was performed at 6/24/48 hours to detect fluorescence for each organ. The results suggested that the liver was the main site for non-specific accumulation of fluorescence ($P < 0.05$), but the signal was considerably decreased

after 24 hours ($P < 0.05$) (Fig. 3-27). (6hrs sample n = 3, 24hrs sample n = 3, 48hrs sample n = 3)

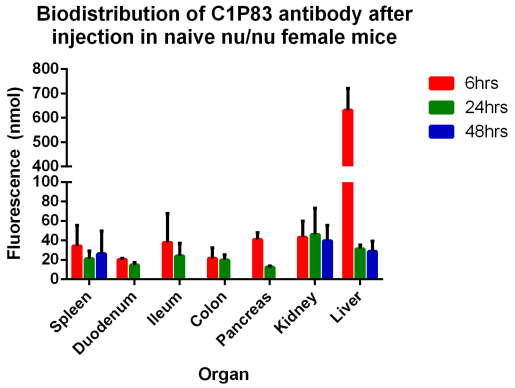

Fig.3-27 Biological distribution of ex vivo NIR fluorescence (6/24/48 hours)

Histological study:

In the therapeutic setting, the limited localization and penetration of monoclonal antibodies into solid tumors restricts their antitumor efficacy. Pancreatic adenocarcinoma cells grow in fibrotic stroma abundant in extracellular matrix components, mostly collagen, and the stroma is poorly perfused. To characterize perfusion and fibrosis of the BxPC3 tumor, staining for blood vessels and fibrosis was performed.

Evaluation of microvessel density (MVD, CD31) and fibrous collagen status of the orthotopic tumors showed that the MVD and fibrous interstitial substance of xenografted tumors were abundant. It indicated that this experimental tumor tissues had good vascular permeability and the potential for therapeutic delivery of drugs by the antibody. (Fig. 3-28; Fig. 3-29; Fig. 3-30)

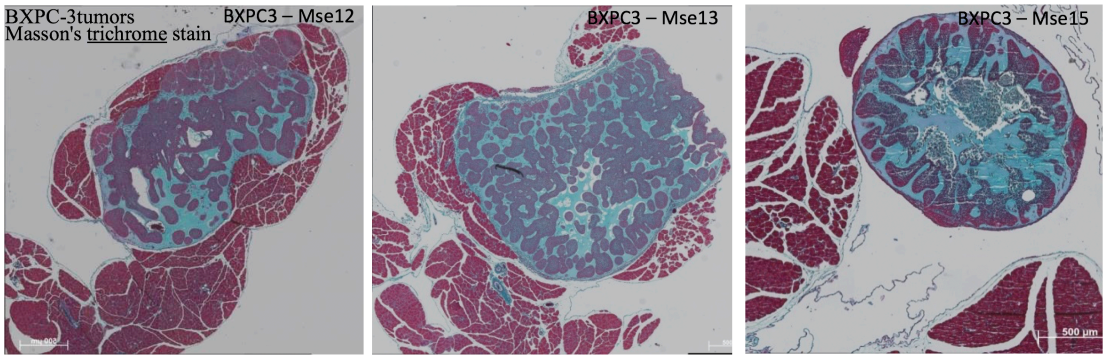

Fig.3-28 Masson's trichrome stain method to evaluate the state of neoplastic fibrous interstitial in tumors (blue-green indicated fibrous tissue composition)

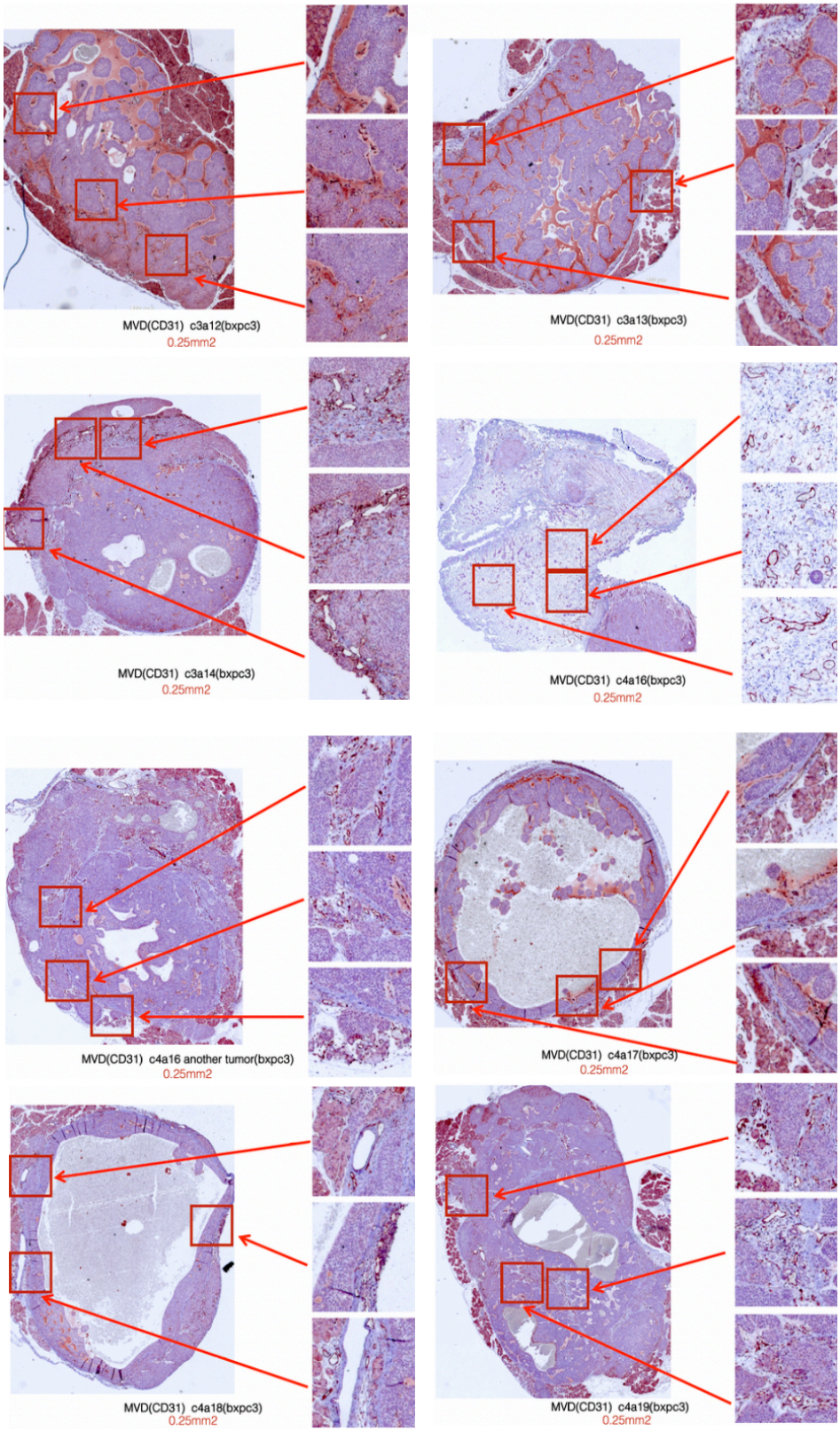

Fig.3-29 Evaluation of MVD of pancreatic tumor after NIR fluorescent imaging (0.25 mm^2)

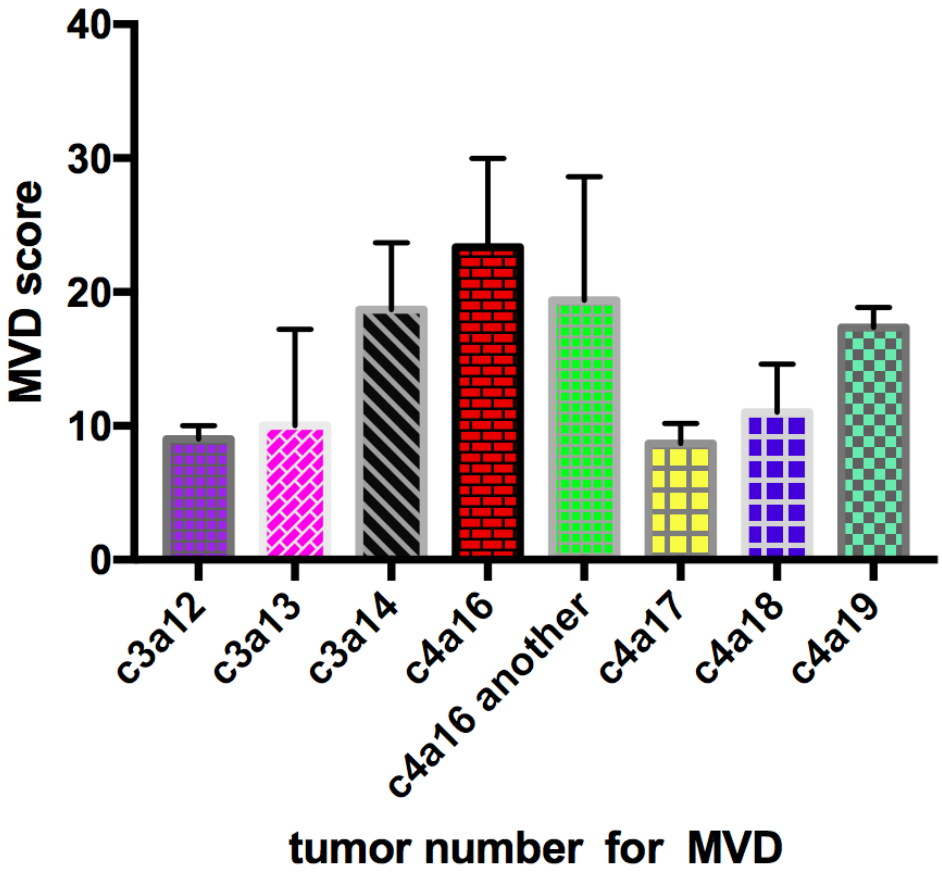

Fig.3-30 Evaluation of MVD after NIR fluorescence imaging of pancreatic orthotopic tumors

(7) Detection of small tumors or metastasis: NIR fluorescent molecular imaging

To test the sensitivity of the antibody in detecting micro-metastasis, the bulk of the tumor was resected under white light but a visible small pocket of tumor was left unresected. Following resection, the mice injected with the labelled antibody were imaged later to determine if the small unresected residual tumor could be detected. Upon detection, the residual tumor was subsequently removed and imaged again to reveal a tumor free abdomen. (Fig.3-31)

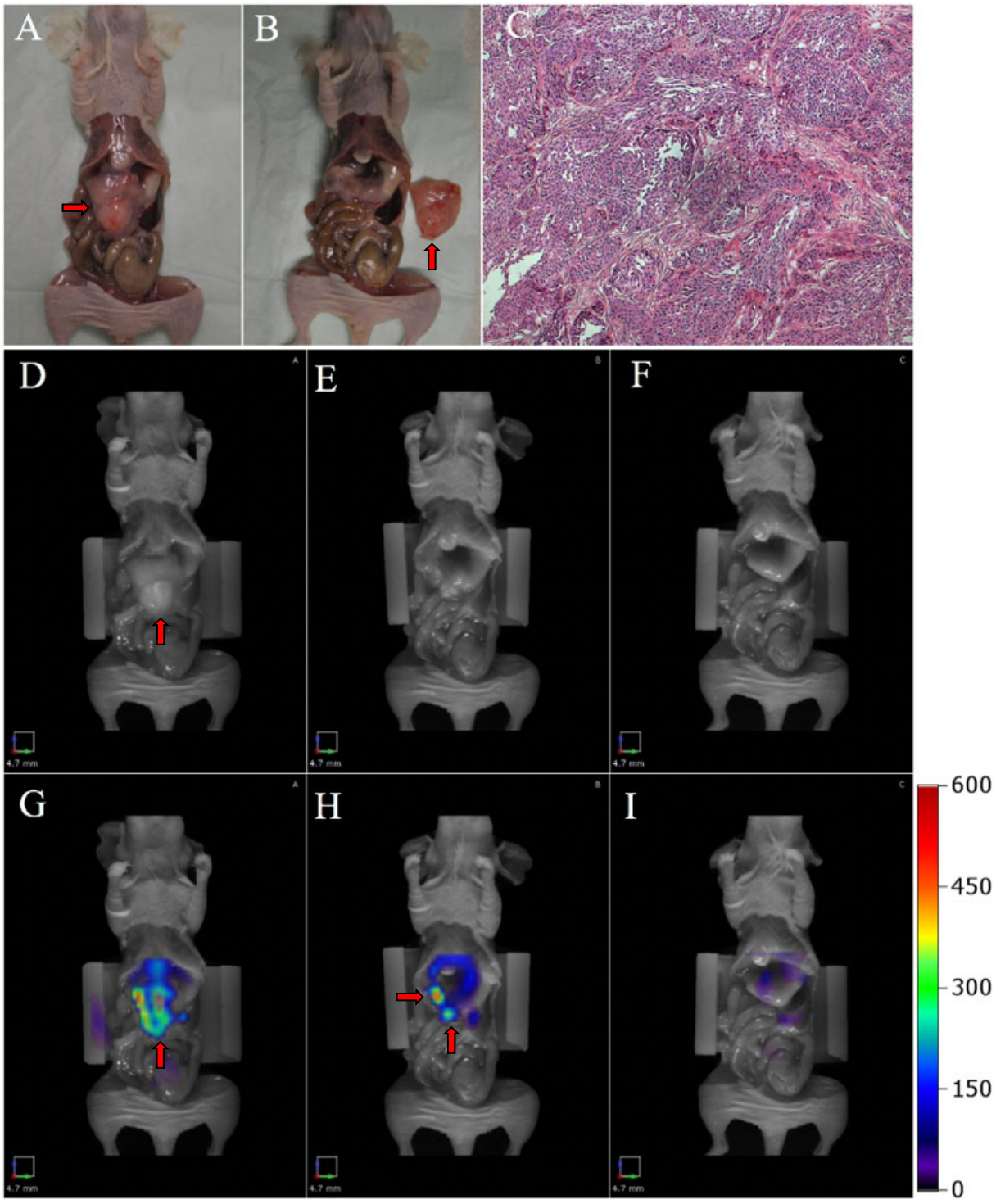

Fig.3-31 NIR fluorescent imaging could find micrometastasis of the tumor (1)

A: tumor in vivo status; B: tumor removal status; C: pathological confirmation; D: tumor in vivo status in FMT2500; E: micrometastasis in vivo in FMT2500; F: micrometastasis removal status in FMT2500; G: tumor in vivo status by NIR fluorescence imaging in FMT2500; H: micrometastasis in vivo status by NIR fluorescence imaging in FMT2500 (pathologically confirmed); I: NIR fluorescent imaging after micrometastasis removed; (Arrows indicate)

4. Discussion

In the study, we demonstrated the feasibility of CEACAM5 targeted NIR fluorescent molecular imaging in a xenografted immunodeficiency mouse model of pancreatic cancer by a novel monoclonal antibody C1P83 labeled with IRDye800CW. The monoclonal antibody C1P83 targets CEACAM5 at epitope GOLD 3 (Hammarstrom et al., 1989). By a controlled antibody of IgG, the specificity and sensitivity of detection was tested and the in vivo distribution of nonspecific signal was verified. Additionally, the xenografted tumor model showed that C1P83-IRDye800CW was able to find tiny tumors or micro-metastasis, which indicated its potential specific diagnostic value and surgical navigation application in the near future.

	KRAS	**TP53**	**P16/CDKN2A**	**SMAD4**
BxPC3	WT	Mutation	Mutation(product absent)	Mutation
PANC-1	Mutation	Mutation	Deletion (product absent)	WT

Table 4-1 Genotype of pancreatic cell line between BxPC3 and Panc1.

In the present study, the chosen pancreatic cancer cell lines were BxPC3 and Panc1. Originally, BxPC-3 cell line was cultured from an old female pancreatic adenocarcinoma of the body and expressed carcinoembryonic antigen with a moderate differentiation in phenotype. While PANC-1 cell line was cultured from an invading pancreatic adenocarcinoma of the head and did not express carcinoembryonic antigen with a poor differentiation in phenotype. Genotype of these two cell lines are listed in Table 4-1 and the relationship of genotye and phenotype remains unclear as the studies to assess the relation of such mutations and cell behavior are too few(Deer et al., 2010). KRAS mutations seem to be the most common mutation in pancreatic cancer, and most available pancreatic cancer cell lines have KRAS mutations except BxPC-3 cell line. For examples, both CAPAN-1 and PANC-1 cell lines have KRAS mutations, but CAPAN-1 cells express CEACAM5 while PANC-1 cells do not express

CEACAM-5. The negative expression of carcinoembryonic antigen in PANC-1 may be correlated with multiple epigenetic alterations and the detail mechanism of this heterogenicity remains unclear. (Deer et al., 2010)

Human CEACAM-5 was regarded as a poor prognostic factor in human digestive cancers; and some reported that CEACAM-5 positive BxPC-3 cells have higher tumorigenicity in tumor size than that of CEACAM-5 negative PANC-1 cells (Aubert et al., 2003; Miknyoczki et al., 1999), while some reported the opposite results (Fukasawa and Korc, 2004) which indicated that the correlation between CEACAM-5 expression and pancreatic tumor growth remains inconclusive. In our subcutaneous model we found an interesting fact that the size of MC38 (CEACAM-5 negative) subcutaneous tumor was much greater than that of C15A3 (CEACAM-5 positive, transfected with human CEACAM-5), however the exact mechanism was unclear and needs to be further investigated.

CEACMA5 was not only the target for fluorescence imaging, but also may serve as a therapeutic target. Reyes et al reported that multi-drug resistant cancer cells will be sensitive to the T cell bispecific antibody cibisatamab (CEA-TCB) which binds CEACAM5 on cancer cells and CD3 on T cells by pharmaceutically increasing CEA expression with WNT inhibitors (Gonzalez-Exposito et al., 2019). Interestingly, some other pharmacological agents such as 5-fluorouracil, interleukins or interferons may also cause the up-regulation of CEACAM5 expression (Aquino et al., 2004). This may have potential clinical interest relevant to cancer diagnosis and therapy for monoclonal antibody or tumor vaccines targeting CEACAM5 (Klein et al., 2017).

In the present study, we found that the higher concentration resulted in higher tumor-to-background ratio. Though the difference was not significant, our explanation is that it might due to limited samples. As C1P83 is an intact antibody which cannot be removed rapidly in vivo, too high concentration of antibody may also result in unacceptable background. Optimization seems necessary before translating into human application in the future. Another interesting phenomenon is that we found that the fluorescent signal could last for nearly one week, which might provide a promising target for immunotherapy.

Concerning the ratio of dye to protein for fluorescent imaging, some reported that 5:1 molar ratio of dye to protein was optimal for NIR fluorescent conjugation(Meincke et al., 2011). Some reported that the fluorescence intensity increased in parallel with higher dye to protein ratio as for the dye of IRDye800CW(Aldrich et al., 2011). In our preliminary study, stronger fluorescent signal could be achieved for higher dye to protein ratio within the range of 1-5:1. Over-labeling with higher dye to protein than 5:1 may result in high background, thus the sensitivity and specificity may be decreased. In prevention of distorted absorption spectrum, the final dye to protein ratio was about 2:1 for purified conjugates for in vivo imaging.

It was believed that fibrous nature of pancreatic tumor interfered with antibody targeting diagnosis and therapy, while our tumor model of BxPC cell in mice indicated good vascular permeability, which is comparable with the literature; and both BxPC-3 and Capan-1 cell lines showed high angiogenic potential, while AsPC-1 and MIA PaCa-2 cell lines had low levels of angiogenic potential (Deer et al., 2010). However, this experimental tumor is different with the humanized tumor regarding the fibrosis, angiogenic potential and microenvironment, a patient-derived xenograft (PDX) model is required to test the novel antibody of C1P83.

Compared with previous fluorescent imaging studies targeting epitope 1 of CEACAM5 by humanized M5A mAb developed from T84.66, the time of peak fluorescent intensity and the TBR are similar with the present study (Lwin et al., 2018). Another study reported similar TBR of about 5 at 72 hours postinjection with single-chain anti-body fragment (Boonstra et al., 2015). And Studies of fluorescent imaging by C1P83 have not been reported by other authors. It indicated that further studies with multiple cell lines and mouse model should be performed and evaluated.

Although the current results of this study are encouraging, our technology model is limited by the large molecular weight of intact antibodies and the only partial humanization of imaging models. Firstly, intact antibodies stay in the circulation longer (1-3 weeks), which gives them sufficient time to accumulate in the tumor. However, this means that it also takes several days for the fluorescent background of blood and normal organs to be removed, which makes them unsuitable as radiolabeled probes. The cycle time of a complete monoclonal antibody is

relatively long, and many research teams have evaluated it in clinical immunoPET studies over the years (Wu and Olafsen, 2008). Due to its long residence time in the blood, high non-specific background signals may hinder the diagnostic potential of intact antibodies (Sharkey et al., 2010; Wu and Olafsen, 2008). Therefore, combining the recombinant antibody fragments (F(ab′)2, Fab, ScFv, and sdAb) with fluorescent probes directly for NIR fluorescent molecular imaging may greatly improve the imaging efficiency and back-to-ground ratio. The low immunogenicity of antibody fragments will also improve the safety of imaging. Secondly, the preclinical animal models have their limitations. Most current studies are performed on immunodeficiency animals. For human CEACAM5 targeted imaging, immunodeficient mice models are probably not adequate because rodents lack the gene of human CEACAM5. Consequently, the binding of the antibody to normal epithelium is unknown and the specific tumor signal is artificially augmented. (Chevinsky, 1991). Thirdly, the xenograft model using cancer cell lines is not sufficient to represent the complex heterogeneity of human tumor, and it could not reflect the patient's response sufficiently. Moreover, the xenograft tumor often cannot recapitulate the tumor microenvironment and how the microenvironment will influence the fluorescent molecular imaging remains unknown. To overcome these limitations, a PDX model seems necessary as a more advanced preclinical cancer model. Fourthly, the model of micro-metastases detection was not performed in various pancreatic cancer cell lines and has not been verified in PDX tumor model. Moreover, the detection was performed after laparotomy with the main tumor removed, and the micro-metastases were not in the liver. For liver metastases, its signal may be masked by the liver signal due to the hydrophobicity of the IDye800CW, despite that the masking fluorescence would decrease rapidly to baseline within 12-48 hours. Thus, it's diagnostic potential in vivo for hepatic micro-metastases need to be further evaluated in liver metastasis models by comparison of MRI and fluorescent imaging.

And for outlook, we envisage the following three directions mainly.

First, The next generation of animal models. the In order to establish a more humanized animal model, CEABAC2 transgenic mice have been obtained, originally developed by Dr Clifford Stanners, from the Morris Goodman Cancer Center(Chan et al., 2006), The transgene

consists of a genomic insertion of two copies of intact 187 kb artificial human bacterial chromosomes (BAC) that contain most of the proximal human CEACAMs gene cluster. The CEABAC2 mice are genetically of the fvb strain and immunocompetent, so only tumor cell lines originated from the fvb strain could be inoculated into the CEABAC2 mice. We will use this "humanized" animal model to compare the binding of smaller FAB fragment of the antibody C1P83.

Second, Development of next-generation antibodies. Develop antibody fragments of CEACAM5 monoclonal antibody C1P83 through genetic engineering, and combine antibody fragments (F(ab′)2, Fab, ScFv, and sdAb) directly with fluorescent probes for in vivo NIR fluorescent molecular imaging may greatly improve imaging efficiency and tumor-to-background ratio. Reducing the immunogenicity of antibody fragments will also improve the safety of imaging. The monoclonal antibody recombinant fragment targeting CEACAM5 antigen epitope GOLD 3 may have further application prospects. If I^{123} can be coupled to C1P83 recombinant antibody fragments, it is expected to develop targeted SPECT diagnosis and treatment methods; if I^{131} or drug-containing liposomes or nanomaterials can be coupled to C1P83 recombinant antibody fragments, it is also expected to develop A new model of targeted therapy for pancreatic cancer.

Third, The next generation of NIR-II fluorescent molecular imaging probes. Compared with the NIR-I spectrum of 700-900 nm, the tumor-to-background ratio and fluorescent imaging quality in the NIR-II spectrum of 1000-1700 nm are significantly improved (Diao et al., 2015). The advantages of NIR-II nanoprobes are obvious: due to the long emission wavelength, low scattering, photon absorption is almost negligible, and autofluorescence is also reduced to the lowest range (Hong et al., 2015). Therefore, the tissue penetration of NIR-II nanoprobe is better, and it has higher spatiotemporal resolution and deeper imaging depth in biological tissue imaging (Ding et al., 2018). Currently, popular NIR-II nanoprobes are single-walled carbon nanotubes, rare-earth ion-doped nanocrystals, semiconductor quantum dots, small organic molecular materials, and conjugated polymers.

Small organic molecules can be designed and adjusted with fine spectroscopic properties, have high biocompatibility, fast excretion ability, simple and fast preparation methods, and have important advantages in molecular design based on the NIR-II region. Considering the application of NIR-II region imaging agents in clinical applications, probes based on small organic molecules are still the best candidate. Therefore, the development of NIR-II region probes based on small organic molecules is currently a hot area of research. (Antaris et al., 2016; Antaris et al., 2017; Cosco et al., 2017; Feng et al., 2017; Li et al., 2018a; Shou et al., 2017; Sun et al., 2017; Sun et al., 2016; Sun et al., 2018; Zhu et al., 2017).

To date, only two NIRF probes, IRDye800CW and ICG, have passed safety tests and are allowed to be used clinically (Whitley et al., 2016). If the NIR-II spectrum fluorescent probe can be bound to C1P83 or its recombinant antibody fragment, combined with multimodal tumor molecular imaging is expected to accelerate the transformation of this project from bench to bedside.

5. Summary

CEACAM5 is a potential molecular target for visualization and localization of CEACAM5 expressing cancers by NIR (NIR) fluorescence imaging. We synthesized conjugates of CEACAM5 monoclonal antibody C1P83 (targeting epitope Gold 3 of human CEACAM5) with NIR fluorescent dye of IRDye800CW. Purified conjugates of C1P83-IRDye800CW were tested for binding selectivity in vitro of human BxPC-3 cancer cells that express CEACAM5, and the Binding was time-dependent. Conjugates failed to label the PANC-1 cells which is a CEACAM5 negative control. In the subcutaneous tumor model in immunodeficient mice, subcutaneously inoculated tumors of C15A3 cells, which express CEACAM5, were visualized with high sensitivity. In the orthotopic pancreatic model, C1P83-conjugates can be applied for visualization of the orthotopic pancreatic tumor. Results of ex vivo were comparable to those obtained in vivo. Overall, fluorescent conjugates of C1P83-IRDye800CW were sensitive for detection of pancreas cancer by targeting CEACAM5.

In conclusion, fluorescent C1P83-IRDye800CW conjugates were sensitive and selective for NIR fluorescent detection of pancreatic cancer by targeting CEACAM5. The CEACAM5 epitope GOLD 3 is a potential molecular target for NIR fluorescent molecular imaging. This NIR fluorescent imaging modality based on the monoclonal antibody of C1P83 is expected to evolve into future fluorescent surgical navigation .

6. References

Albers, G.H., Fleuren, G., Escribano, M.J., and Nap, M. (1988). Immunohistochemistry of CEA in the human pancreas during development, in the adult, chronic pancreatitis, and pancreatic adenocarcinoma. American journal of clinical pathology *90*, 17-22.

Aldrich, M.B., Wang, X., Hart, A., Kwon, S., Sampath, L., Marshall, M.V., and Sevick-Muraca, E.M. (2011). Assessment of free dye in solutions of dual-labeled antibody conjugates for in vivo molecular imaging. Mol Imaging Biol *13*, 32-42.

Allum, W.H., Stokes, H.J., Macdonald, F., and Fielding, J.W. (1986). Demonstration of carcinoembryonic antigen (CEA) expression in normal, chronically inflamed, and malignant pancreatic tissue by immunohistochemistry. Journal of clinical pathology *39*, 610-614.

Antaris, A.L., Chen, H., Cheng, K., Sun, Y., Hong, G., Qu, C., Diao, S., Deng, Z., Hu, X., Zhang, B.*, et al.* (2016). A small-molecule dye for NIR-II imaging. Nat Mater *15*, 235-242.

Antaris, A.L., Chen, H., Diao, S., Ma, Z., Zhang, Z., Zhu, S., Wang, J., Lozano, A.X., Fan, Q., Chew, L.*, et al.* (2017). A high quantum yield molecule-protein complex fluorophore for near-infrared II imaging. Nat Commun *8*, 15269.

Aquino, A., Formica, V., Prete, S.P., Correale, P.P., Massara, M.C., Turriziani, M., De Vecchis, L., and Bonmassar, E. (2004). Drug-induced increase of carcinoembryonic antigen expression in cancer cells. Pharmacol Res *49*, 383-396.

Aubert, M., Crotte, C., Bernard, J.P., Lombardo, D., Sadoulet, M.O., and Mas, E. (2003). Decrease of human pancreatic cancer cell tumorigenicity by alpha1,3galactosyltransferase gene transfer. Int J Cancer *107*, 910-918.

Beauchemin, N., Draber, P., Dveksler, G., Gold, P., Gray-Owen, S., Grunert, F., Hammarstrom, S., Holmes, K.V., Karlsson, A., Kuroki, M.*, et al.* (1999). Redefined nomenclature for members of the carcinoembryonic antigen family. Experimental cell research *252*, 243-249.

Bharali, D.J., and Mousa, S.A. (2010). Emerging nanomedicines for early cancer detection and improved treatment: current perspective and future promise. Pharmacology & therapeutics *128*, 324-335.

Bjerner, J., Lebedin, Y., Bellanger, L., Kuroki, M., Shively, J.E., Varaas, T., Nustad, K., Hammarstrom, S., and Bormer, O.P. (2002). Protein epitopes in carcinoembryonic antigen. Report of the ISOBM TD8 workshop. Tumour biology : the journal of the International Society for Oncodevelopmental Biology and Medicine *23*, 249-262.

Boonstra, M.C., Tolner, B., Schaafsma, B.E., Boogerd, L.S., Prevoo, H.A., Bhavsar, G., Kuppen, P.J., Sier, C.F., Bonsing, B.A., Frangioni, J.V*., et al.* (2015). Preclinical evaluation of a novel CEA-targeting near-infrared fluorescent tracer delineating colorectal and pancreatic tumors. Int J Cancer *137*, 1910-1920.
Chan, C.H., Cook, D., and Stanners, C.P. (2006). Increased colon tumor susceptibility in azoxymethane treated CEABAC transgenic mice. Carcinogenesis *27*, 1909-1916.

Chevinsky, A.H. (1991). CEA in tumors of other than colorectal origin. Seminars in surgical oncology *7*, 162-166.

Cosco, E.D., Caram, J.R., Bruns, O.T., Franke, D., Day, R.A., Farr, E.P., Bawendi, M.G., and Sletten, E.M. (2017). Flavylium Polymethine Fluorophores for Near- and Shortwave Infrared Imaging. Angew Chem Int Ed Engl *56*, 13126-13129.

Deer, E.L., Gonzalez-Hernandez, J., Coursen, J.D., Shea, J.E., Ngatia, J., Scaife, C.L., Firpo, M.A., and Mulvihill, S.J. (2010). Phenotype and genotype of pancreatic cancer cell lines. Pancreas *39*, 425-435.
DeVita VT, H.S., Rosenberg SA (2005). Cancer, principles & practice of oncology. Philadelphia: Lippincott Williams & Wilkins *7*.

Diao, S., Blackburn, J.L., Hong, G., Antaris, A.L., Chang, J., Wu, J.Z., Zhang, B., Cheng, K., Kuo, C.J., and Dai, H. (2015). Fluorescence Imaging In Vivo at Wavelengths beyond 1500 nm. Angew Chem Int Ed Engl *54*, 14758-14762.

Ding, F., Zhan, Y., Lu, X., and Sun, Y. (2018). Recent advances in near-infrared II fluorophores for multifunctional biomedical imaging. Chem Sci *9*, 4370-4380.

Fass, L. (2008). Imaging and cancer: a review. Molecular oncology *2*, 115-152.

Feng, Y., Zhu, S., Antaris, A.L., Chen, H., Xiao, Y., Lu, X., Jiang, L., Diao, S., Yu, K., Wang, Y*., et al.* (2017). Live imaging of follicle stimulating hormone receptors in gonads and bones using near infrared II fluorophore. Chem Sci *8*, 3703-3711.

Frangioni, J.V. (2003). In vivo near-infrared fluorescence imaging. Current opinion in chemical biology *7*, 626-634.

Frangioni, J.V. (2008). New technologies for human cancer imaging. Journal of clinical oncology : official journal of the American Society of Clinical Oncology *26*, 4012-4021.

Fukasawa, M., and Korc, M. (2004). Vascular endothelial growth factor-trap suppresses tumorigenicity of multiple pancreatic cancer cell lines. Clin Cancer Res *10*, 3327-3332.

Gioux, S., Choi, H.S., and Frangioni, J.V. (2010). Image-guided surgery using invisible near-infrared light: fundamentals of clinical translation. Mol Imaging *9*, 237-255.

Gold, P., and Freedman, S.O. (1965). Specific carcinoembryonic antigens of the human digestive system. The Journal of experimental medicine *122*, 467-481.

Gonzalez-Exposito, R., Semiannikova, M., Griffiths, B., Khan, K., Barber, L.J., Woolston, A., Spain, G., von Loga, K., Challoner, B., Patel, R.*, et al.* (2019). CEA expression heterogeneity and plasticity confer resistance to the CEA-targeting bispecific immunotherapy antibody cibisatamab (CEA-TCB) in patient-derived colorectal cancer organoids. J Immunother Cancer *7*, 101.

Hammarstrom, S. (1999). The carcinoembryonic antigen (CEA) family: structures, suggested functions and expression in normal and malignant tissues. Seminars in cancer biology *9*, 67-81.

Hammarstrom, S., Shively, J.E., Paxton, R.J., Beatty, B.G., Larsson, A., Ghosh, R., Bormer, O., Buchegger, F., Mach, J.P., Burtin, P.*, et al.* (1989). Antigenic sites in carcinoembryonic antigen. Cancer Res *49*, 4852-4858.

He, X., Gao, J., Gambhir, S.S., and Cheng, Z. (2010). Near-infrared fluorescent nanoprobes for cancer molecular imaging: status and challenges. Trends in molecular medicine *16*, 574-583.

Hefta, L.J., Neumaier, M., and Shively, J.E. (1998). Kinetic and affinity constants of epitope specific anti-carcinoembryonic antigen (CEA) monoclonal antibodies for CEA and engineered CEA domain constructs. Immunotechnology : an international journal of immunological engineering *4*, 49-57.

Hilderbrand, S.A., and Weissleder, R. (2010). Near-infrared fluorescence: application to in vivo molecular imaging. Current opinion in chemical biology *14*, 71-79.

Hinoda, Y., Neumaier, M., Hefta, S.A., Drzeniek, Z., Wagener, C., Shively, L., Hefta, L.J., Shively, J.E., and Paxton, R.J. (1988). Molecular cloning of a cDNA coding biliary glycoprotein I: primary structure of a glycoprotein immunologically crossreactive with carcinoembryonic antigen. Proceedings of the National Academy of Sciences of the United States of America *85*, 6959-6963.

Hiroshima, Y., Maawy, A., Metildi, C.A., Zhang, Y., Uehara, F., Miwa, S., Yano, S., Sato, S., Murakami, T., Momiyama, M.*, et al.* (2014). Successful fluorescence-guided surgery on human colon cancer patient-derived orthotopic xenograft mouse models using a fluorophore-conjugated anti-CEA antibody and a portable imaging system. J Laparoendosc Adv Surg Tech A *24*, 241-247.

Hong, G., Diao, S., Antaris, A.L., and Dai, H. (2015). Carbon Nanomaterials for Biological Imaging and Nanomedicinal Therapy. Chem Rev *115*, 10816-10906.

Klein, C., Waldhauer, I., Nicolini, V.G., Freimoser-Grundschober, A., Nayak, T., Vugts, D.J., Dunn, C., Bolijn, M., Benz, J., Stihle, M.*, et al.* (2017). Cergutuzumab amunaleukin (CEA-IL2v), a CEA-targeted IL-2 variant-based immunocytokine for combination cancer immunotherapy: Overcoming limitations of aldesleukin and conventional IL-2-based immunocytokines. Oncoimmunology *6*, e1277306.

Kovar, J.L., Simpson, M.A., Schutz-Geschwender, A., and Olive, D.M. (2007). A systematic approach to the development of fluorescent contrast agents for optical imaging of mouse cancer models. Analytical biochemistry *367*, 1-12.

Li, B., Lu, L., Zhao, M., Lei, Z., and Zhang, F. (2018a). An Efficient 1064 nm NIR-II Excitation Fluorescent Molecular Dye for Deep-Tissue High-Resolution Dynamic Bioimaging. Angew Chem Int Ed Engl *57*, 7483-7487.

Li, H., Wang, P., Gong, W., Wang, Q., Zhou, J., Zhu, W.H., and Cheng, Y. (2018b). Dendron-Grafted Polylysine-Based Dual-Modal Nanoprobe for Ultra-Early Diagnosis of Pancreatic Precancerosis via Targeting a Urokinase-Type Plasminogen Activator Receptor. Adv Healthc Mater *7*.

Luo, H., England, C.G., Goel, S., Graves, S.A., Ai, F., Liu, B., Theuer, C.P., Wong, H.C., Nickles, R.J., and Cai, W. (2017). ImmunoPET and Near-Infrared Fluorescence Imaging of Pancreatic Cancer with a Dual-Labeled Bispecific Antibody Fragment. Mol Pharm *14*, 1646-1655.

Lwin, T.M., Murakami, T., Miyake, K., Yazaki, P.J., Shivley, J.E., Hoffman, R.M., and Bouvet, M. (2018). Tumor-Specific Labeling of Pancreatic Cancer Using a Humanized Anti-CEA Antibody Conjugated to a Near-Infrared Fluorophore. Ann Surg Oncol *25*, 1079-1085.

Mahmood, U., and Weissleder, R. (2003). Near-infrared optical imaging of proteases in cancer. Molecular cancer therapeutics *2*, 489-496.

Markov, P., Satoi, S., and Kon, M. (2016). Redefining the R1 resection in patients with pancreatic ductal adenocarcinoma. J Hepatobiliary Pancreat Sci *23*, 523-532.

Meincke, M., Tiwari, S., Hattermann, K., Kalthoff, H., and Mentlein, R. (2011). Near-infrared molecular imaging of tumors via chemokine receptors CXCR4 and CXCR7. Clin Exp Metastasis *28*, 713-720.

Metildi, C.A., Kaushal, S., Luiken, G.A., Hoffman, R.M., and Bouvet, M. (2014). Advantages of fluorescence-guided laparoscopic surgery of pancreatic cancer labeled with fluorescent anti-carcinoembryonic antigen antibodies in an orthotopic mouse model. J Am Coll Surg *219*, 132-141.

Metildi, C.A., Kaushal, S., Snyder, C.S., Hoffman, R.M., and Bouvet, M. (2013). Fluorescence-guided surgery of human colon cancer increases complete resection resulting in cures in an orthotopic nude mouse model. J Surg Res *179*, 87-93.

Miknyoczki, S.J., Chang, H., Klein-Szanto, A., Dionne, C.A., and Ruggeri, B.A. (1999). The Trk tyrosine kinase inhibitor CEP-701 (KT-5555) exhibits significant antitumor efficacy in preclinical xenograft models of human pancreatic ductal adenocarcinoma. Clin Cancer Res *5*, 2205-2212.

Nap, M., Hammarstrom, M.L., Bormer, O., Hammarstrom, S., Wagener, C., Handt, S., Schreyer, M., Mach,

J.P., Buchegger, F., von Kleist, S.*, et al.* (1992). Specificity and affinity of monoclonal antibodies against carcinoembryonic antigen. Cancer Res *52*, 2329-2339.

Neesse, A., Hahnenkamp, A., Griesmann, H., Buchholz, M., Hahn, S.A., Maghnouj, A., Fendrich, V., Ring, J., Sipos, B., Tuveson, D.A.*, et al.* (2013). Claudin-4-targeted optical imaging detects pancreatic cancer and its precursor lesions. Gut *62*, 1034-1043.

Ntziachristos, V. (2006). Fluorescence molecular imaging. Annual review of biomedical engineering *8*, 1-33.

Nurunnabi, M., Cho, K.J., Choi, J.S., Huh, K.M., and Lee, Y.K. (2010). Targeted near-IR QDs-loaded micelles for cancer therapy and imaging. Biomaterials *31*, 5436-5444.

Ogawa, M., Kosaka, N., Choyke, P.L., and Kobayashi, H. (2009). In vivo molecular imaging of cancer with a quenching near-infrared fluorescent probe using conjugates of monoclonal antibodies and indocyanine green. Cancer Res *69*, 1268-1272.

Pysz, M.A., Gambhir, S.S., and Willmann, J.K. (2010). Molecular imaging: current status and emerging strategies. Clinical radiology *65*, 500-516.

RP., H. (2002.). Molecular probes. . handbook of fluorescent probes and research chemicals 9th ed Eugene, OR: Molecular Probes Inc; .

Schmiegel, W.H., Kalthoff, H., Arndt, R., Gieseking, J., Greten, H., Kloppel, G., Kreiker, C., Ladak, A., Lampe, V., and Ulrich, S. (1985). Monoclonal antibody-defined human pancreatic cancer-associated antigens. Cancer Res *45*, 1402-1407.

Sharkey, R.M., Rossi, E.A., Chang, C.H., and Goldenberg, D.M. (2010). Improved cancer therapy and molecular imaging with multivalent, multispecific antibodies. Cancer biotherapy & radiopharmaceuticals *25*, 1-12.

Shively, J.E., and Beatty, J.D. (1985). CEA-related antigens: molecular biology and clinical significance. Critical reviews in oncology/hematology *2*, 355-399.

Shou, K., Qu, C., Sun, Y., Chen, H., Chen, S., Zhang, L., Xu, H., Hong, X., Yu, A., and Cheng, Z. (2017). Multifunctional biomedical imaging in physiological and pathological conditions using a NIR-II probe. Adv Funct Mater *27*.

Siegel, R.L., Miller, K.D., and Jemal, A. (2019). Cancer statistics, 2019. CA Cancer J Clin *69*, 7-34.

Strobel, O., Hank, T., Hinz, U., Bergmann, F., Schneider, L., Springfeld, C., Jager, D., Schirmacher, P., Hackert, T., and Buchler, M.W. (2017). Pancreatic Cancer Surgery: The New R-status Counts. Ann Surg

265, 565-573.

Sun, Y., Ding, M., Zeng, X., Xiao, Y., Wu, H., Zhou, H., Ding, B., Qu, C., Hou, W., Er-Bu, A.*, et al.* (2017). Novel bright-emission small-molecule NIR-II fluorophores for in vivo tumor imaging and image-guided surgery. Chem Sci *8*, 3489-3493.

Sun, Y., Qu, C., Chen, H., He, M., Tang, C., Shou, K., Hong, S., Yang, M., Jiang, Y., Ding, B.*, et al.* (2016). Novel benzo-bis(1,2,5-thiadiazole) fluorophores for in vivo NIR-II imaging of cancer. Chem Sci *7*, 6203-6207.

Sun, Y., Zeng, X., Xiao, Y., Liu, C., Zhu, H., Zhou, H., Chen, Z., Xu, F., Wang, J., Zhu, M.*, et al.* (2018). Novel dual-function near-infrared II fluorescence and PET probe for tumor delineation and image-guided surgery. Chem Sci *9*, 2092-2097.

Trajkovic-Arsic, M., Mohajerani, P., Sarantopoulos, A., Kalideris, E., Steiger, K., Esposito, I., Ma, X., Themelis, G., Burton, N., Michalski, C.W.*, et al.* (2014). Multimodal molecular imaging of integrin alphavbeta3 for in vivo detection of pancreatic cancer. J Nucl Med *55*, 446-451.

Uehara, F., Hiroshima, Y., Miwa, S., Tome, Y., Yano, S., Yamamoto, M., Matsumoto, Y., Maehara, H., Tanaka, K., Bouvet, M.*, et al.* (2015). Fluorescence-guided surgery of retroperitoneal-implanted human fibrosarcoma in nude mice delays or eliminates tumor recurrence and increases survival compared to bright-light surgery. PLoS One *10*, e0116865.

von Kleist, S., Chavanel, G., and Burtin, P. (1972). Identification of an antigen from normal human tissue that crossreacts with the carcinoembryonic antigen. Proceedings of the National Academy of Sciences of the United States of America *69*, 2492-2494.

Wang, H., Huff, T.B., Zweifel, D.A., He, W., Low, P.S., Wei, A., and Cheng, J.X. (2005). In vitro and in vivo two-photon luminescence imaging of single gold nanorods. Proceedings of the National Academy of Sciences of the United States of America *102*, 15752-15756.

Weissleder, R., and Ntziachristos, V. (2003). Shedding light onto live molecular targets. Nature medicine *9*, 123-128.

Whitley, M.J., Cardona, D.M., Lazarides, A.L., Spasojevic, I., Ferrer, J.M., Cahill, J., Lee, C.L., Snuderl, M., Blazer, D.G., 3rd, Hwang, E.S.*, et al.* (2016). A mouse-human phase 1 co-clinical trial of a protease-activated fluorescent probe for imaging cancer. Sci Transl Med *8*, 320ra324.

Will, O.M., Purcz, N., Chalaris, A., Heneweer, C., Boretius, S., Purcz, L., Nikkola, L., Ashammakhi, N., Kalthoff, H., Gluer, C.C.*, et al.* (2016). Increased survival rate by local release of diclofenac in a murine model of recurrent oral carcinoma. Int J Nanomedicine *11*, 5311-5321.

Willmann, J.K., Chen, K., Wang, H., Paulmurugan, R., Rollins, M., Cai, W., Wang, D.S., Chen, I.Y., Gheysens, O., Rodriguez-Porcel, M.*, et al.* (2008a). Monitoring of the biological response to murine hindlimb ischemia with 64Cu-labeled vascular endothelial growth factor-121 positron emission tomography. Circulation *117*, 915-922.

Willmann, J.K., Cheng, Z., Davis, C., Lutz, A.M., Schipper, M.L., Nielsen, C.H., and Gambhir, S.S. (2008b). Targeted microbubbles for imaging tumor angiogenesis: assessment of whole-body biodistribution with dynamic micro-PET in mice. Radiology *249*, 212-219.

Willmann, J.K., Lutz, A.M., Paulmurugan, R., Patel, M.R., Chu, P., Rosenberg, J., and Gambhir, S.S. (2008c). Dual-targeted contrast agent for US assessment of tumor angiogenesis in vivo. Radiology *248*, 936-944.
Willmann, J.K., Paulmurugan, R., Chen, K., Gheysens, O., Rodriguez-Porcel, M., Lutz, A.M., Chen, I.Y., Chen, X., and Gambhir, S.S. (2008d). US imaging of tumor angiogenesis with microbubbles targeted to vascular endothelial growth factor receptor type 2 in mice. Radiology *246*, 508-518.

Wu, A.M., and Olafsen, T. (2008). Antibodies for molecular imaging of cancer. Cancer journal *14*, 191-197.

Yamaguchi, K., Enjoji, M., and Tsuneyoshi, M. (1991). Pancreatoduodenal carcinoma: a clinicopathologic study of 304 patients and immunohistochemical observation for CEA and CA19-9. Journal of surgical oncology *47*, 148-154.

Yang, L., Mao, H., Cao, Z., Wang, Y.A., Peng, X., Wang, X., Sajja, H.K., Wang, L., Duan, H., Ni, C.*, et al.* (2009). Molecular imaging of pancreatic cancer in an animal model using targeted multifunctional nanoparticles. Gastroenterology *136*, 1514-1525 e1512.

Yano, S., Miwa, S., Kishimoto, H., Toneri, M., Hiroshima, Y., Yamamoto, M., Bouvet, M., Urata, Y., Tazawa, H., Kagawa, S.*, et al.* (2015a). Experimental Curative Fluorescence-guided Surgery of Highly Invasive Glioblastoma Multiforme Selectively Labeled With a Killer-reporter Adenovirus. Mol Ther *23*, 1182-1188.
Yano, S., Miwa, S., Kishimoto, H., Uehara, F., Tazawa, H., Toneri, M., Hiroshima, Y., Yamamoto, M., Urata, Y., Kagawa, S.*, et al.* (2015b). Targeting tumors with a killer-reporter adenovirus for curative fluorescence-guided surgery of soft-tissue sarcoma. Oncotarget *6*, 13133-13148.

Yano, S., Takehara, K., Kishimoto, H., Urata, Y., Kagawa, S., Bouvet, M., Fujiwara, T., and Hoffman, R.M. (2016). Adenoviral targeting of malignant melanoma for fluorescence-guided surgery prevents recurrence in orthotopic nude-mouse models. Oncotarget *7*, 18558-18572.

Yano, S., Zhang, Y., Miwa, S., Kishimoto, H., Urata, Y., Bouvet, M., Kagawa, S., Fujiwara, T., and Hoffman, R.M. (2015c). Precise navigation surgery of tumours in the lung in mouse models enabled by in situ fluorescence labelling with a killer-reporter adenovirus. BMJ Open Respir Res *2*, e000096.

Zhu, S., Yang, Q., Antaris, A.L., Yue, J., Ma, Z., Wang, H., Huang, W., Wan, H., Wang, J., Diao, S.*, et al.*

(2017). Molecular imaging of biological systems with a clickable dye in the broad 800- to 1,700-nm near-infrared window. Proc Natl Acad Sci U S A *114*, 962-967.

7. Acknowledgements

First of all, I would like to express my deepest gratitude to my supervisor, Prof. Dr rer. nat. Holger Kalthoff, for his scientific guidance, for his sage advice, for his insightful criticism, for his enthusiastic help, and for his patient encouragement. There is no proper word to express my sincere gratitude.

Deepest gratitude also goes to Dr. Sanjay Tiwari for his great support throughout this study, particularly for his very scientific supervision and intensive discussion in details. This research project would not have been possible without his kind encouragement and patient instruction.

Many thanks to Prof. Claus-Christian Glüer, Prof. Dr. Susanne Sebens, Prof. Jan-Bernd Hövener, Christian Röder, Robert Tower, Matina Jansen, Stefan Reinhold, Oula Peñate Medina, Reinhild Holmer, Jaime Andrés Peña, Lukas Huber, Petra Fademrecht ……

Finally, I want express my gratitude to my family, and my colleagues in Hangzhou for their huge support.